

INFORMATION TO USERS

The most advanced technology has been used to photograph and reproduce this manuscript from the microfilm master. UMI films the text directly from the original or copy submitted. Thus, some thesis and dissertation copies are in typewriter face, while others may be from any type of computer printer.

The quality of this reproduction is dependent upon the quality of the copy submitted. Broken or indistinct print, colored or poor quality illustrations and photographs, print bleedthrough, substandard margins, and improper alignment can adversely affect reproduction.

In the unlikely event that the author did not send UMI a complete manuscript and there are missing pages, these will be noted. Also, if unauthorized copyright material had to be removed, a note will indicate the deletion.

Oversize materials (e.g., maps, drawings, charts) are reproduced by sectioning the original, beginning at the upper left-hand corner and continuing from left to right in equal sections with small overlaps. Each original is also photographed in one exposure and is included in reduced form at the back of the book. These are also available as one exposure on a standard 35mm slide or as a 17" x 23" black and white photographic print for an additional charge.

Photographs included in the original manuscript have been reproduced xerographically in this copy. Higher quality 6" x 9" black and white photographic prints are available for any photographs or illustrations appearing in this copy for an additional charge. Contact UMI directly to order.

U·M·I

University Microfilms International
A Bell & Howell Information Company
300 North Zeeb Road, Ann Arbor, MI 48106-1346 USA
313/761-4700 800/521-0600

Order Number 1337439

**Physical and chemical processes affecting forced ventilation of
benzene and *p*-xylene in a desert soil**

Van de Water, James Gordon, M.S.

The University of Arizona, 1989

U·M·I
300 N. Zeeb Rd.
Ann Arbor, MI 48106

PHYSICAL AND CHEMICAL PROCESSES
AFFECTING FORCED VENTILATION OF
BENZENE AND *p*-XYLENE IN A DESERT SOIL

by

James Gordon Van de Water

A Thesis Submitted to the Faculty of the
DEPARTMENT OF HYDROLOGY AND WATER RESOURCES

In Partial Fulfillment of the Requirements
for the Degree of

MASTER OF SCIENCE
WITH A MAJOR IN HYDROLOGY

In the Graduate College

THE UNIVERSITY OF ARIZONA

1 9 8 9

STATEMENT BY AUTHOR

This thesis has been submitted in partial fulfillment of requirements for an advanced degree at The University of Arizona and is deposited in the University Library to be made available to borrowers under rules of the Library.

Brief quotations from this thesis are allowable without special permission, provided that accurate acknowledgement of source is made. Requests for permission for extended quotation from or reproduction of this manuscript in whole or in part may be granted by the head of the major department or the Dean of the Graduate College when in his or her judgement the proposed use of the material is in the interests of scholarship. In all other instances, however, permission must be obtained from the author.

SIGNED: James Gordon Vinde Water

APPROVAL BY THESIS DIRECTORS

This thesis has been approved on the date shown below:

Martha H. Conklin
 Martha H. Conklin
 Assistant Research Hydrologist
 Hydrology and Water Resources

May 12, 1989
 Date

Roger C. Bales
 Roger C. Bales
 Assistant Professor
 Hydrology and Water Resources

May 12, 1989
 Date

ACKNOWLEDGEMENTS

I thank my parents for their support (emotional and financial) throughout my academic career. I couldn't have done it without them. This thesis is dedicated in memory of my father, Harry Van de Water.

This thesis was written under the watchful eye of Dr. Martha Conklin. I thank her for her advice, patience, and the many hours she spent reviewing the manuscript.

I am also indebted to Hal Davis for his advice and sense of humor when things didn't go smoothly.

I thank Dr. Roger Bales for leading me through the maze of mathematical models used for this study.

This project was funded by the Salt River Project, Phoenix, Arizona. I thank them and Dennis Shirley for their support.

TABLE OF CONTENTS

| | <u>Page</u> |
|--|-------------|
| LIST OF ILLUSTRATIONS | 7 |
| LIST OF TABLES | 11 |
| ABSTRACT..... | 13 |
| 1. INTRODUCTION..... | 14 |
| 1.1 Rate-limiting Processes..... | 14 |
| 1.2 Equilibrium Partitioning..... | 17 |
| 1.3 Research Objectives | 19 |
| 2. BACKGROUND | 20 |
| 2.1 Model Development..... | 20 |
| 2.1.1 Two-compartment model..... | 23 |
| 2.1.2 One-site kinetic model | 23 |
| 2.1.3 Slow diffusion model | 24 |
| 2.1.4 Equilibrium model..... | 24 |
| 2.2 Effect of Parameters on Breakthrough Curves..... | 24 |
| 2.3 Non-linear Least Squares Curve-fitting using CFITIM..... | 34 |
| 3. MATERIALS AND METHODS..... | 37 |
| 3.1 Chemicals..... | 37 |
| 3.2 Soil | 37 |
| 3.2.1 Sample Preparation | 37 |
| 3.2.2 Preparation of Soil Columns | 38 |

TABLE OF CONTENTS--Continued

| | <u>Page</u> |
|--|-------------|
| 3.3 Helium Tracer Experiments | 39 |
| 3.3.1 Apparatus | 40 |
| 3.3.2 Experimental Procedure | 40 |
| 3.3.3 Flow Meter Calibration..... | 43 |
| 3.4 Flow versus Pressure Experiments | 48 |
| 3.4.1 Apparatus..... | 49 |
| 3.4.2 Experimental Procedure | 49 |
| 3.4.3 Air Permeability Studies | 49 |
| 3.4.4 Compressible Flow Studies..... | 51 |
| 3.5 Soil Venting Experiments | 53 |
| 3.5.1 Apparatus | 54 |
| 3.5.2 Experimental Procedure | 54 |
| 3.6 Saturated Column Experiments | 59 |
| 4. RESULTS | 60 |
| 4.1 Helium Tracer Experiments | 60 |
| 4.2 Saturated Column Experiment | 69 |
| 4.3 Soil Venting Experiments | 69 |
| 4.3.1 Mass Balances | 71 |
| 4.3.2 Curve-fitting Results | 76 |
| 4.3.2.1 Equilibrium Model | 76 |
| 4.3.2.2 One-site Kinetic Model | 81 |

TABLE OF CONTENTS--Continued

| | <u>Page</u> |
|---|-------------|
| 4.3.2.3 Slow Diffusion Model..... | 87 |
| 4.3.2.4 Two-compartment Model..... | 92 |
| 5. DISCUSSION | 97 |
| 5.1 Helium Tracer Experiments | 97 |
| 5.2 Saturated Column Experiment | 98 |
| 5.3 Soil Venting Experiments | 98 |
| 5.3.1 Mass Balances | 98 |
| 5.3.2 Curve-fitting Results | 100 |
| 6. CONCLUSIONS | 103 |
| APPENDIX A. OBSERVED AND FITTED HELIUM BREAKTHROUGH CURVES | 105 |
| APPENDIX B. OBSERVED AND FITTED BENZENE BREAKTHROUGH CURVES | 111 |
| APPENDIX C. OBSERVED AND FITTED p-XYLENE BREAKTHROUGH CURVES | 116 |
| LIST OF REFERENCES | 119 |

LIST OF ILLUSTRATIONS

| <u>Figure</u> | <u>Page</u> |
|--|-------------|
| 1.1 Conceptual physical-chemical model | 15 |
| 2.2.1 Effect of R on the breakthrough curve | 28 |
| 2.2.2 Effect of P on the breakthrough curve..... | 29 |
| 2.2.3 Effect of T ₁ on the breakthrough curve | 31 |
| 2.2.4 Effect of β on the breakthrough curve | 33 |
| 2.2.5 Effect of ω on the breakthrough curve | 35 |
| 3.3.1 Experimental apparatus used for helium tracer and flow vs. pressure experiments | 41 |
| 3.3.2 Flow meter calibration curves for the wet and dry soil columns | 47 |
| 3.4.1 Darcy velocity vs. pressure | 52 |
| 3.5.1 Experimental apparatus used for soil venting experiments | 55 |
| 4.1.1 Observed and fitted data for experiment H3W using the equilibrium model | 61 |
| 4.1.2 D_d/D_o vs. θ_a based on porous media diffusion models appearing in the literature | 65 |
| 4.1.3 Mechanical dispersion vs. average linear velocity | 68 |
| 4.2.1 Observed and fitted breakthrough curves for experiment SAT2 using the one-site kinetic model of van Genuchten (1981) | 70 |
| 4.3.1 Hypothetical inflow and outflow curves illustrating the method of calculating mass balance from the area under the curves..... | 72 |

LIST OF ILLUSTRATIONS--Continued

| <u>Figure</u> | <u>Page</u> |
|--|-------------|
| 4.3.2 D/D_0 vs. $v_d d/D_0$ for the benzene and <i>p</i> -xylene using the equilibrium model | 80 |
| 4.3.3 Observed and fitted breakthrough curves for wet column experiment B3 using the one-site kinetic model | 83 |
| 4.3.4 Observed and fitted breakthrough curves for dry column experiment B17 using the one-site kinetic model | 84 |
| 4.3.5 Observed and fitted breakthrough curves for wet column experiment XY9 using the one-site kinetic model | 85 |
| 4.3.6 Observed and fitted breakthrough curves for dry column experiment B17 using the slow diffusion model..... | 88 |
| 4.3.7 Observed and fitted breakthrough curves for wet column experiment XY9 using the two-compartment model..... | 95 |
| A.1 Observed and fitted data for experiment H1W using the equilibrium model..... | 106 |
| A.2 Observed and fitted data for experiment H2W using the equilibrium model..... | 106 |
| A.3 Observed and fitted data for experiment H4W using the equilibrium model..... | 107 |
| A.4 Observed and fitted data for experiment H5W using the equilibrium model | 107 |
| A.5 Observed and fitted data for experiment H1D using the equilibrium model | 108 |
| A.6 Observed and fitted data for experiment H2D using the equilibrium model..... | 108 |

LIST OF ILLUSTRATIONS--Continued

| <u>Figure</u> | <u>Page</u> |
|--|-------------|
| A.7 Observed and fitted data for experiment H3D using the equilibrium model | 109 |
| A.8 Observed and fitted data for experiment H4D using the equilibrium model | 109 |
| A.9 Observed and fitted data for experiment H5D using the equilibrium model | 110 |
| B.1 Observed and fitted breakthrough curves for experiment B4 using the one-site kinetic model | 112 |
| B.2 Observed and fitted breakthrough curves for experiment B5 using the one-site kinetic model | 112 |
| B.3 Observed and fitted breakthrough curves for experiment B6 using the one-site kinetic model | 113 |
| B.4 Observed and fitted breakthrough curves for experiment B8 using the one-site kinetic model | 113 |
| B.5 Observed and fitted breakthrough curves for experiment B9 using the one-site kinetic model | 114 |
| B.6 Observed and fitted breakthrough curves for experiment B10 using the one-site kinetic model | 114 |
| B.7 Observed and fitted breakthrough curves for experiment B16 using the one-site kinetic model | 115 |
| B.8 Observed and fitted breakthrough curves for experiment B16 using the slow diffusion model | 115 |
| C.1 Observed and fitted breakthrough curves for experiment XY8 using the one-site kinetic model | 117 |
| C.2 Observed and fitted breakthrough curves for experiment XY10 using the one-site kinetic model | 117 |

LIST OF ILLUSTRATIONS--Continued

| <u>Figure</u> | <u>Page</u> |
|--|-------------|
| C.3 Observed and fitted breakthrough curves for experiment XY8 using the two-compartment model | 118 |
| C.4 Observed and fitted breakthrough curves for experiment XY10 using the two-compartment model | 118 |

LIST OF TABLES

| <u>Table</u> | <u>Page</u> |
|---|-------------|
| 3.3.1 Listing of Helium Tracer Experiments..... | 44 |
| 3.3.2 Flow Meter Calibration Curve Data..... | 46 |
| 3.4.1 Listing of Flow versus Pressure Experiments | 50 |
| 3.5.1 Listing of Soil Venting Experiments..... | 58 |
| 4.1.1 Curve-fitting Results for the Helium Tracer Breakthrough Curve Data using the Equilibrium Model..... | 62 |
| 4.1.2 Porous Media Diffusion Models | 64 |
| 4.1.3 Dispersion, Mechanical Dispersion, and Porous Media Diffusion for the Wet and Dry Soil Columns..... | 67 |
| 4.3.1 Mass Balance Results | 73 |
| 4.3.2 Equilibrium Mass Distribution of Benzene and <i>p</i> -Xylene in the Soil, Aqueous, and Vapor Phases..... | 77 |
| 4.3.3 Curve-fitting Results for the Benzene and <i>p</i> -Xylene Soil Venting Experiments using the Equilibrium Model..... | 79 |
| 4.3.4 Dimensionless Parameters obtained using the One-site Kinetic Model | 82 |
| 4.3.5 Dimensional Partitioning and Kinetic Parameters obtained using the One-site Kinetic Model..... | 86 |
| 4.3.6 Dimensionless Parameters for the Dry Column Benzene Soil Venting Experiments using the Slow Diffusion Model | 89 |
| 4.3.7 Dimensional Partitioning and Kinetic Parameters for the Dry Column Benzene Soil Venting Experiments using the Slow Diffusion Model..... | 91 |

LIST OF TABLES--Continued

| <u>Table</u> | <u>Page</u> |
|--|-------------|
| 4.3.8 Dimensionless Parameters for the Wet Column <i>p</i> -Xylene Soil Venting Experiments using the Two-compartment Model..... | 93 |
| 4.3.9 Dimensional Partitioning and Kinetic Parameters for the Wet Column <i>p</i> -Xylene Soil Venting Experiments using the Two-compartment Model | 96 |

ABSTRACT

The rate at which volatile organic compounds (VOCs) are removed from the vadose zone by forced ventilation may be reduced by slow micro-scale processes such as diffusion through intra-aggregate and pore water and slow reactions at sorption sites located at the soil-water interface. Column experiments using benzene and *p*-xylene were performed in order to simulate cleanup of VOCs in the vadose zone by forced ventilation. Analytical solutions of the one-dimensional advection-dispersion equation coupled to mass transfer equations were fitted to the data. Parameter estimates were used in order to determine time scales of diffusion through water, desorption from, and sorption to, soil organic matter. Lower limits for the time scales for these processes were calculated to be on the order of minutes. Results indicate that these micro-scale processes reduce the rate of removal on the laboratory scale but may have no effect on the field scale.

CHAPTER 1

INTRODUCTION

Petroleum products are frequently stored above the water table in underground storage tanks (USTs). USTs may leak petroleum products to the unsaturated zone due to age or improper installation. Removal of volatile organic compounds (VOCs) of petroleum products in the unsaturated zone can be accomplished by using forced ventilation and vacuum extraction. The maintenance of an undersaturated vapor phase is necessary when removing VOCs by means of forced ventilation and vacuum extraction. Both of these removal techniques have proven to be successful in both field (Crow et al., 1987; Bruckner and Kugele, 1985; and Woodward and Clyde Consultants, 1986) and laboratory experiments (Marley, 1985).

1.1 Rate-limiting Processes

Micro-scale processes controlling the rate of removal of VOCs from the unsaturated zone are evidenced by tailing of breakthrough (removal) curves. A breakthrough curve is a graphical representation of outflow concentration versus time data at a specific location. Tailing of a breakthrough curve results from a slow decline in the concentration as a function of time. Bruckner et al. (1986) suggested that tailing may be the result of volatilization, diffusion through the aqueous phase, and desorption from the soil phase.

Figure 1.1 shows a conceptual model of the unsaturated zone and the different physical and chemical processes which reduce the efficiency of vapor

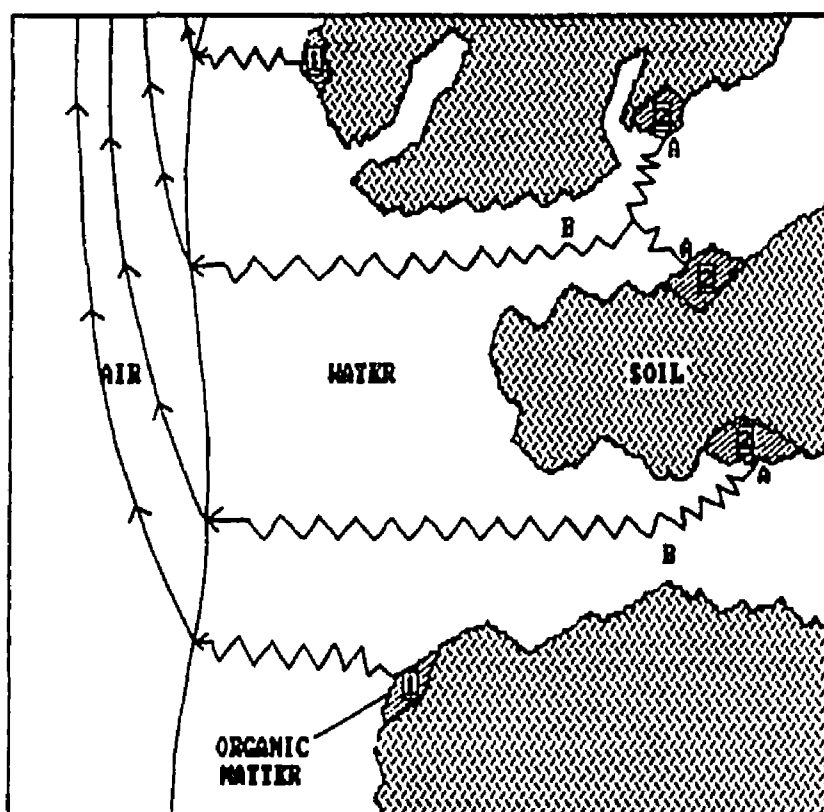


Figure 1.1. Conceptual physical-chemical model.

phase contaminant removal. The system studied involved three phases: (1) a mobile air phase, (2) an immobile water phase, and (3) an immobile solid (soil-organic matter) phase. The organic matter may be further subdivided to include both "fast" sorption sites (site 1 in Figure 1.1), which equilibrate rapidly with the compound in solution and are a relatively short distance from the air-water interface (have a short diffusive path length) and "slow" sorption sites (site 2 in Figure 1.1) which are either kinetically controlled, are relatively far from the air-water interface (have a long diffusive path length), or both.

The two slow processes investigated in this study are illustrated in Figure 1.1: (A) slow release from the sorption site, and (B) slow diffusion through the water. The diffusive path may include both intra- and inter-aggregate channels. One or both of these processes may control the rate of removal.

Szecsody and Bales (in press) found desorption from organic matter to be the rate-limiting step in aqueous phase transport of substituted benzenes in saturated systems. In unsaturated systems, mass must diffuse through water before reaching the air-water interface. Long diffusive path lengths, which might occur at higher moisture contents, may result in diffusion being a rate-limiting step. Wu and Gschwend (1988) developed a numerical model for saturated systems in which intra-aggregate diffusion through water was combined with sorption to the particle surface in order to describe non-equilibrium exchange between the soil and water. Observed tailing was successfully reproduced for systems in which the particle size distribution was narrow. Szecsody and Bales (in press) found that slow diffusion through immobile pore water accounted for some

of the observed tailing in breakthrough curves involving substituted benzenes in saturated systems. Slow diffusion through the sorbent (organic matter bound to the soil aggregates) may also reduce the efficiency of cleanup if the diffusive path length is long.

1.2 Equilibrium Partitioning

Equilibrium partitioning of VOCs between the aqueous and vapor phases is described by Henry's Law:

$$C_a = K_H C_w \quad (1.2.1)$$

where C_a = vapor phase concentration (mg/cm³ air); C_w = aqueous phase concentration (mg/cm³ water); and K_H = Henry's constant (cm³ water/cm³ air). This relationship holds for ideal (dilute) solutions. Since most organic compounds present in gasoline are relatively insoluble in water, Henry's Law describes the air-water partitioning at equilibrium. For this study, the values used for the K_H of benzene and *p*-xylene were 0.23 and 0.29 cm³ water/cm³ air, respectively (Mackay and Shiu, 1981) at 20°C.

Equilibrium partitioning between the water and soil phase can be described by a partition coefficient which is an equilibrium constant representing the distribution of mass in the sorbed and aqueous phases (Eqn. 1.2.2).

$$K_p = C_s/C_w \quad (1.2.2)$$

where K_p = soil-water partition coefficient (cm^3 water/ cm^3 soil); and C_s = concentration in soil phase (mg/cm^3 soil).

K_p is typically reported as cm^3 water/g soil. Conversion to the units given in Eqn. 1.2.2 is accomplished using the density of soil which is assumed to be the same as that of quartz sand (2.65 g soil/ cm^3 soil).

Sorption is the result of partitioning to organic matter bound to the soil aggregates (soil organic matter). Karickhoff et al. (1979) developed the following correlation:

$$K_p = K_{oc}f_{oc} \quad (1.2.3)$$

where K_{oc} (cm^3 water/gram carbon) is the partition coefficient between water and a sorbing phase composed entirely of organic carbon.

K_p , and hence the degree to which a compound will sorb, is inversely related to the solubility of the compound. The hydrophobicity of a compound is indirectly related to its solubility and polarity and may be quantified by the octanol-water partition coefficient (K_{ow}). Schwarzenbach and Westall (1981) found the following linear relation for benzene and substituted benzenes in soils having f_{oc} greater than 0.001:

$$\log K_{oc} = 0.72 \log K_{ow} + 0.49 \quad (1.2.4)$$

Substitution of Eqn. 1.2.3 into Eqn. 1.2.4 gives:

$$\log K_p = 0.72 \log K_{ow} + \log f_{oc} + 0.49 \quad (1.2.5)$$

Eqn. 1.2.5 indicates that K_p is both compound- and soil-dependent.

1.3 Research Objectives

The purpose of this research was to identify the predominant micro-scale processes controlling removal of VOCs during forced ventilation.

Breakthrough curves obtained from soil column experiments involving benzene and *p*-xylene (both of which are found in gasoline) were analyzed in order to determine the predominant rate-limiting processes during forced ventilation. The slow processes considered in this thesis were slow desorption from soil organic matter and slow diffusion through water to the air-water interface. Initial concentration, pressure-induced vapor velocity, and moisture content were the experimental variables.

A series of flow versus pressure experiments were performed on two soil columns having different moisture contents in order to determine the respective air permeability (k_a) values. The flow versus pressure data were also used to determine the nature of the flow (i.e., whether flow was compressible or incompressible). Soil column experiments using helium as a conservative tracer yielded breakthrough curves which were analyzed in order to determine the degree of dispersive and diffusive transport for both columns.

CHAPTER 2

BACKGROUND

For this study, four advection-dispersion, partitioning models with different rate-limiting steps were considered for the movement of VOCs in unsaturated soil systems. In these models, two types of soil sites ('fast' and 'slow') were considered. Fast sites (site 1 in Figure 1.1) are assumed to approach equilibrium rapidly, and slow sites (site 2 in Figure 1.1) are assumed to approach equilibrium slowly.

- (1) Two-compartment model: assumes that a fraction of the mass is bound to fast sites while the rest is bound to slow sites;
- (2) One-site kinetic model: assumes that binding and release at all sorption sites are slow and the time scale of diffusion through the water is short;
- (3) Slow diffusion model: assumes that binding and release at all sorption sites are fast and the time scale of diffusion through the water is long; and
- (4) Equilibrium model: assumes that binding and release at all sorption sites are fast and the time scale of diffusion through the water is short;

2.1 Model Development

Breakthrough curves can be described mathematically by the advection-dispersion equation (Eqn. 2.1.1) coupled to one or more equations which describe

the rate-limiting steps.

$$\theta_a \frac{\partial C_a}{\partial t} + \theta_w \frac{\partial C_w}{\partial t} + (1 - \theta_a - \theta_w) \frac{\partial C_{s1}}{\partial t} + (1 - \theta_a - \theta_w) \frac{\partial C_{s2}}{\partial t} = D \theta_a \frac{\partial^2 C_a}{\partial x^2} - v_a \theta_a \frac{\partial C_a}{\partial x} \quad (2.1.1)$$

where θ_a = air-filled porosity (cm^3 air/ cm^3 porous media); θ_w = moisture content (cm^3 water/ cm^3 porous media); $(1 - \theta_a - \theta_w)$ = soil fraction (cm^3 soil/ cm^3 porous media). C_a is the outflow air phase concentration (mg/cm^3 air), C_w = aqueous phase concentration (mg/cm^3 water); C_{s1} = sorbed concentration at the fast sites (mg/cm^3 soil); and C_{s2} = sorbed concentration at the slow sites (mg/cm^3 soil). The sum of C_{s1} and C_{s2} is the total sorbed concentration (C_s). D is the dispersion coefficient (cm^2/sec); v_a = average linear velocity (cm/sec); t = time (sec); and x = distance (cm).

The four terms on the lefthand side of Eqn. 2.1.1 describe changes in mass in the three phases present: air (C_a), water (C_w), and soil (C_{s1} and C_{s2}), that arise from the processes described by the two terms on the righthand side of the equation, dispersion and advection.

Use of Eqn. 2.1.1 assumes the dispersive and advective properties of the system to be constant with respect to time and location. The latter assumption implies steady-state flow. For vapor-phase flow to be at steady state, the pressure at all points in the system must be constant through time.

If the system is at equilibrium, $dC_w/dt = 0$, and Eqn. 1.2.2 can be used to describe partitioning between the sorbed and aqueous phases.

In non-equilibrium conditions, slow diffusion through water can be described as a mass-transfer process:

$$\frac{\partial C_w}{\partial t} = \alpha_w \left(\frac{C_a}{K_H} - C_w \right) \quad (2.1.2)$$

where α_w = mass transfer coefficient (sec^{-1}); and K_H = Henry's constant (cm^3 water/ cm^3 air).

Binding and release at the slow sites can also be described as a mass-transfer process:

$$\frac{\partial C_{s2}}{\partial t} = k_b ([1-F] K_p C_w - C_{s2}) \quad (2.1.3)$$

where F = mass fraction of contaminant sorbed to the fast sites; and k_b = desorption rate coefficient (sec^{-1}). The additional parameter F is required since only a fraction of the sorbed mass resides on the slow sites.

Binding and release at the fast sites is an equilibrium process:

$$\frac{\partial C_{s1}}{\partial t} = F K_p \frac{\partial C_w}{\partial t} \quad (2.1.4)$$

This equation is the time differential form of Eqn. 1.2.2.

2.1.1 Two-compartment Model

The two-compartment model is governed by Eqn. 2.1.1 coupled to Eqn. 2.1.3. This model does not make a distinction between the effects of a slow reaction at the soil site and slow diffusion; thus, the effective rate coefficients obtained using this model represent a combination of these processes. Combining Eqns. 2.1.1, 2.1.4, and 1.2.1, the following equation is obtained;

$$\left(1 + \frac{\theta_w}{\theta_a} \frac{1}{K_H} + F \frac{(1-\theta_a-\theta_w)}{\theta_a}\right) \frac{\partial C_a}{\partial t} + \frac{(1-\theta_a-\theta_w)}{\theta_a} \frac{\partial C_{s2}}{\partial t} = D \frac{\partial^2 C_a}{\partial x^2} - v_a \frac{\partial C_a}{\partial x} \quad (2.1.5)$$

2.1.2 One-site Kinetic Model

The one-site kinetic model is governed by Eqn. 2.1.3 with $F = 0$ ($C_{s2} = C_s$) and Henry's Law.

$$\frac{\partial C_w}{\partial t} = \frac{1}{K_H} \frac{\partial C_a}{\partial t} \quad (2.1.6)$$

This equation describes fast diffusion through the water and is the time differential form of Henry's Law (Eqn 1.2.1). After substitution, the governing equations reduce to:

$$\left(1 + \frac{\theta_w}{\theta_a} \frac{1}{K_H}\right) \frac{\partial C_a}{\partial t} + \frac{(1-\theta_a-\theta_w)}{\theta_a} \frac{\partial C_s}{\partial t} = D \frac{\partial^2 C_a}{\partial x^2} - v_a \frac{\partial C_a}{\partial x} \quad (2.1.7)$$

$$\frac{\partial C_s}{\partial t} = k_b (K_p C_w - C_s) \quad (2.1.8)$$

2.1.3 Slow Diffusion Model

This model is governed by Eqn. 2.1.1 with $C_{s2} = 0$ and Eqn. 2.1.2. Upon substitution of Eqns. 2.1.4 and 2.1.6 into Eqn. 2.1.1, the advection-dispersion equation becomes:

$$\frac{\partial C_a}{\partial t} + \left(\frac{\theta_w}{\theta_a} + \frac{(1-\theta_a-\theta_w)}{\theta_a} K_p \right) \frac{\partial C_w}{\partial t} = D \frac{\partial^2 C_a}{\partial x^2} - v_a \frac{\partial C_a}{\partial x} \quad (2.1.9)$$

2.1.4 Equilibrium Model

Since the equilibrium model does not contain a slow process, equilibrium expressions (Eqns. 1.2.1 and 1.2.2) can be substituted into the lefthand side of Eqn. 2.1.1 leaving only one governing equation. Therefore, the governing equation for the equilibrium model is:

$$\left(1 + \frac{\theta_w}{\theta_a} \frac{1}{K_H} + \frac{(1-\theta_a-\theta_w)}{\theta_a} \frac{K_p}{K_H} \right) \frac{\partial C_a}{\partial t} = D \frac{\partial^2 C_a}{\partial x^2} - v_a \frac{\partial C_a}{\partial x} \quad (2.1.10)$$

2.2 Effect of Parameters on Breakthrough Curves

Dimensional variables which appear in governing equations are often converted to dimensionless variables in order to identify the significance of

related processes. Substitution of dimensionless variables into the kinetic and equilibrium models reduces the governing equations to the following dimensionless equations, for which there are analytical solutions for the appropriate boundary conditions (De Smedt and Wierenga, 1979). The kinetic models (i.e., the two-compartment, one-site kinetic, and slow diffusion models) take the form of Eqns. 2.2.1 and 2.2.2 when expressed in terms of dimensionless variables.

$$R\beta \frac{\partial C_1}{\partial T} + R(1-\beta) \frac{\partial C_2}{\partial T} = \frac{1}{P} \frac{\partial^2 C_1}{\partial z^2} - \frac{\partial C_1}{\partial z} \quad (2.2.1)$$

$$R(1-\beta) \frac{\partial C_2}{\partial T} = \omega(C_1 - C_2) \quad (2.2.2)$$

The dimensionless form of the equilibrium model is:

$$R \frac{\partial C_1}{\partial T} = \frac{1}{P} \frac{\partial^2 C_1}{\partial z^2} - \frac{\partial C_1}{\partial z} \quad (2.2.3)$$

C_1 is the air phase concentration normalized by the influent air phase concentration C_0 :

$$C_1 = C_a / C_0 \quad (2.2.4)$$

where C_0 is expressed in units of mg/cm^3 air.

The dimensionless length scale (z) is defined as the distance traveled (x) relative to the length of the column:

$$z = x/L \quad (2.2.5)$$

where L = column length (cm).

The kinetic models describe a single slow process and therefore require an extra parameter (C_2) which accounts for the rate-limiting process as well as the phase affected. For the two-compartment model:

$$C_2 = C_{s2}/[(1-F)(K_p/K_H)C_o] \quad (2.2.6)$$

for the one-site kinetic model:

$$C_2 = C_s/[(K_p/K_H)C_o] \quad (2.2.7)$$

for the slow diffusion model:

$$C_2 = C_w/(C_o/K_H) \quad (2.2.8)$$

The parameter R is the retardation factor which quantifies the increase in time taken for the VOCs to move through the soil column as a result of partitioning between the mobile (vapor) and immobile (aqueous and soil) phases.

For the two-compartment, slow diffusion, and equilibrium models, R is:

$$R = 1 + \frac{\theta_w}{\theta_a} \frac{1}{K_H} + \frac{(1-\theta_a-\theta_w)}{\theta_a} \frac{K_P}{K_H} \quad (2.2.9)$$

Because of restrictions in the analytical solution to the one-site kinetic model, R takes a different form:

$$R = 1 + \frac{(1-\theta_a-\theta_w)}{K_H\theta_a+\theta_w} K_P \quad (2.2.10)$$

Since partitioning from the mobile phase increases the time taken for a compound to break through, retardation (an increase in R) causes the breakthrough curve to be shifted to the right (Figure 2.2.1). This breakthrough time is referred to as the residence time (t_{rs}) and is defined as the time taken for 50 percent of the input mass to break through at a measurement point.

The parameter P is the Peclet number which is the ratio of the advective length scale to the dispersive length scale of the system.

$$P = v_1 L / D \quad (2.2.11)$$

Dispersion results in a broadening of the breakthrough curve; therefore, a decrease in P serves to broaden the breakthrough curve (Figure 2.2.2).

The dimensionless time scale (T) is defined relative to the flow rate and the physical dimensions of the column:

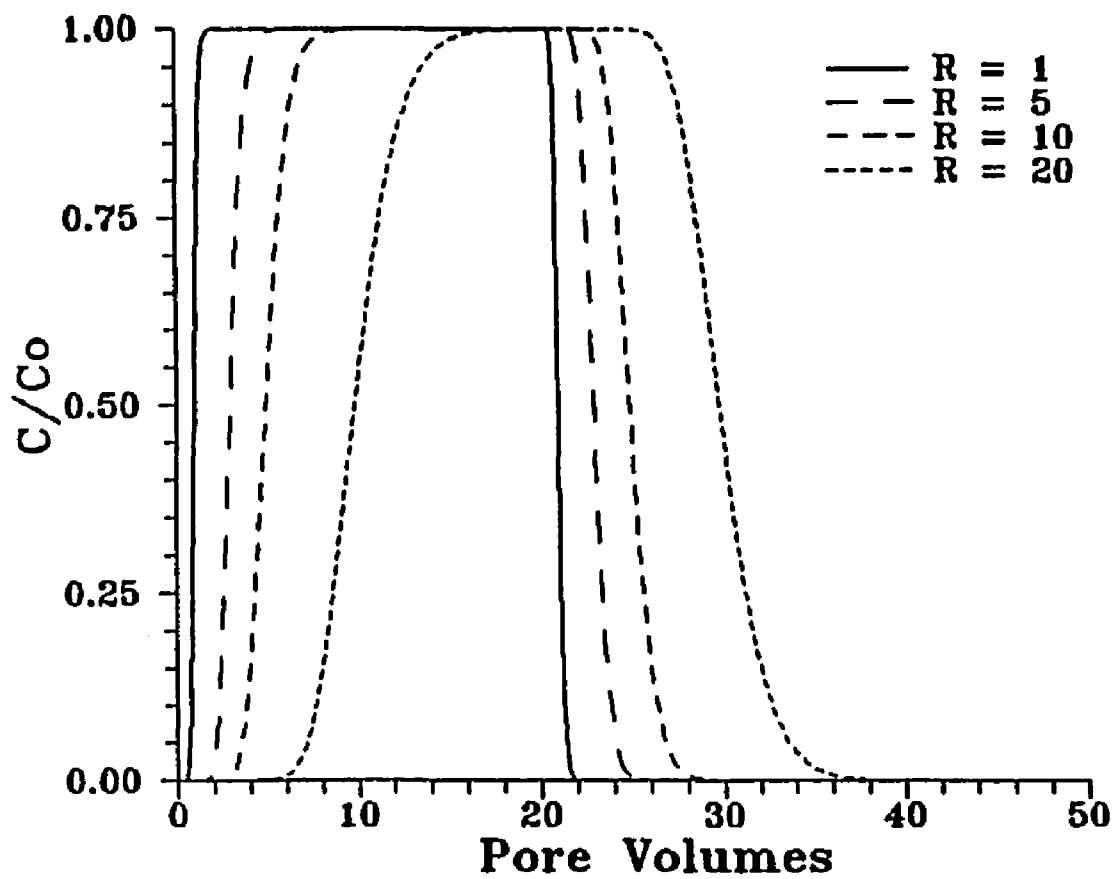


Figure 2.2.1. Effect of R on the breakthrough curve. Breakthrough curves represent equilibrium systems with $P = 50$ and $T_1 = 20$ (see following text for definitions of P and T_1).

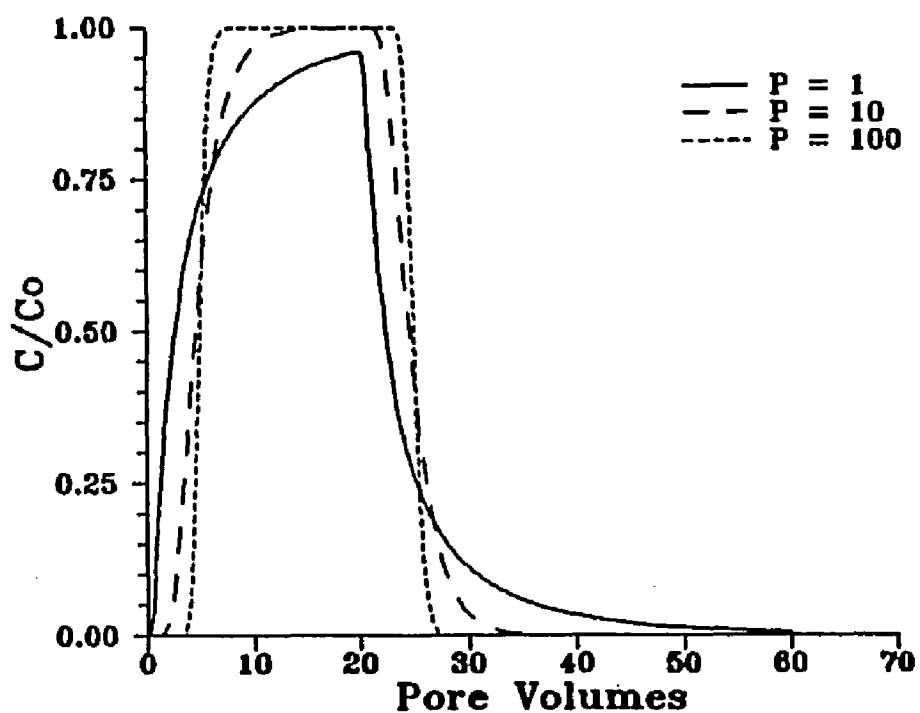


Figure 2.2.2. Effect of P on the breakthrough curve. Breakthrough curves represent equilibrium systems with $R = 5$ and $T_1 = 20$ (see following text for definition of T_1).

$$T = v_a t / L = Qt / L \theta_a A \quad (2.2.12)$$

where Q is the volumetric flow rate (cm^3/sec); and A is the cross-sectional area (cm^2) normal to flow. T is the number of air-filled pore volumes eluted.

Because of restrictions in the analytical solution, T is expressed for the one-site kinetic model as follows:

$$T = v_a t / L(1 + \theta_w / K_H \theta_a) \quad (2.2.13)$$

T_1 is the dimensionless input time and is referred to as the pulse. T_1 represents the number of pore volumes containing the VOCs introduced into the system. The algebraic expression for T_1 is identical to T . Figure 2.2.3 shows the effect of T_1 on the breakthrough curve.

For the two-compartment model, the variable β takes on positive values less than or equal to 1. $\beta = 1.0$ results when all of the sorbed mass is on fast sites (i.e., $F = 1.0$), and no tailing of the breakthrough curve is observed. The minimum β occurs when $F = 0$.

$$\beta = \frac{1 + \frac{\theta_w}{\theta_a} \frac{1}{K_H} + F \frac{(1 - \theta_a - \theta_w)}{\theta_a} \frac{K_P}{K_H}}{1 + \frac{\theta_w}{\theta_a} + \frac{(1 - \theta_a - \theta_w)}{\theta_a} \frac{K_P}{K_H}} \quad (2.2.14)$$

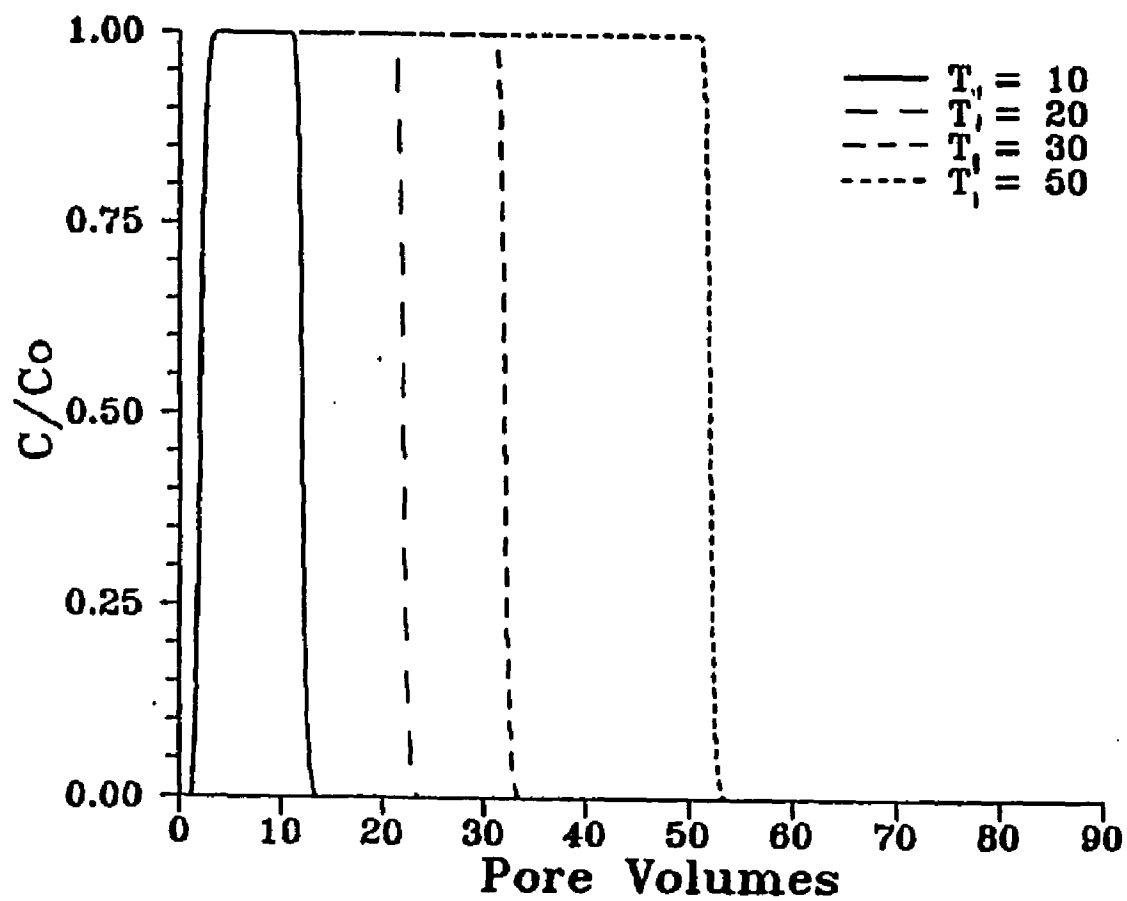


Figure 2.2.3. Effect of T_1 on the breakthrough curve. Breakthrough curves represent equilibrium systems with $R = 2$ and $P = 50$.

which is:

$$\beta = \frac{1 + \frac{\theta_w}{\theta_a} \frac{1}{K_H} + F \frac{(1 - \theta_a - \theta_w)}{\theta_a} \frac{K_p}{K_H}}{R} \quad (2.2.15)$$

A decrease in β will result from a decrease in F . This implies that as β decreases, the extent to which the system is controlled by a non-equilibrium process increases (assuming that the system is known to be subject to a non-equilibrium process). As β decreases, the amount of tailing increases (see Figure 2.2.4).

For the one-site kinetic and slow diffusion models, β is $1/R$ and is therefore not an additional variable.

ω , which appears in the dimensionless rate equation (Eqn. 2.2.2), is the ratio of the physical (advective) time scale to the micro-scale (reaction and/or diffusion) time scale. ω is analogous to the Damkohler number (Bahr and Rubin, 1987). Therefore, $\omega = k_t t_{res} = k_t L / v_a$. When using the two-compartment model to estimate k_f , ω must be normalized by $(1-F)$. For the two-compartment model:

$$\omega = k_b \frac{L}{v_a} R (1 - \beta) \quad (2.2.16)$$

For the one-site kinetic model:

$$\omega = k_b \frac{L}{v_a} (R - 1) \quad (2.2.17)$$

For the the slow diffusion model:

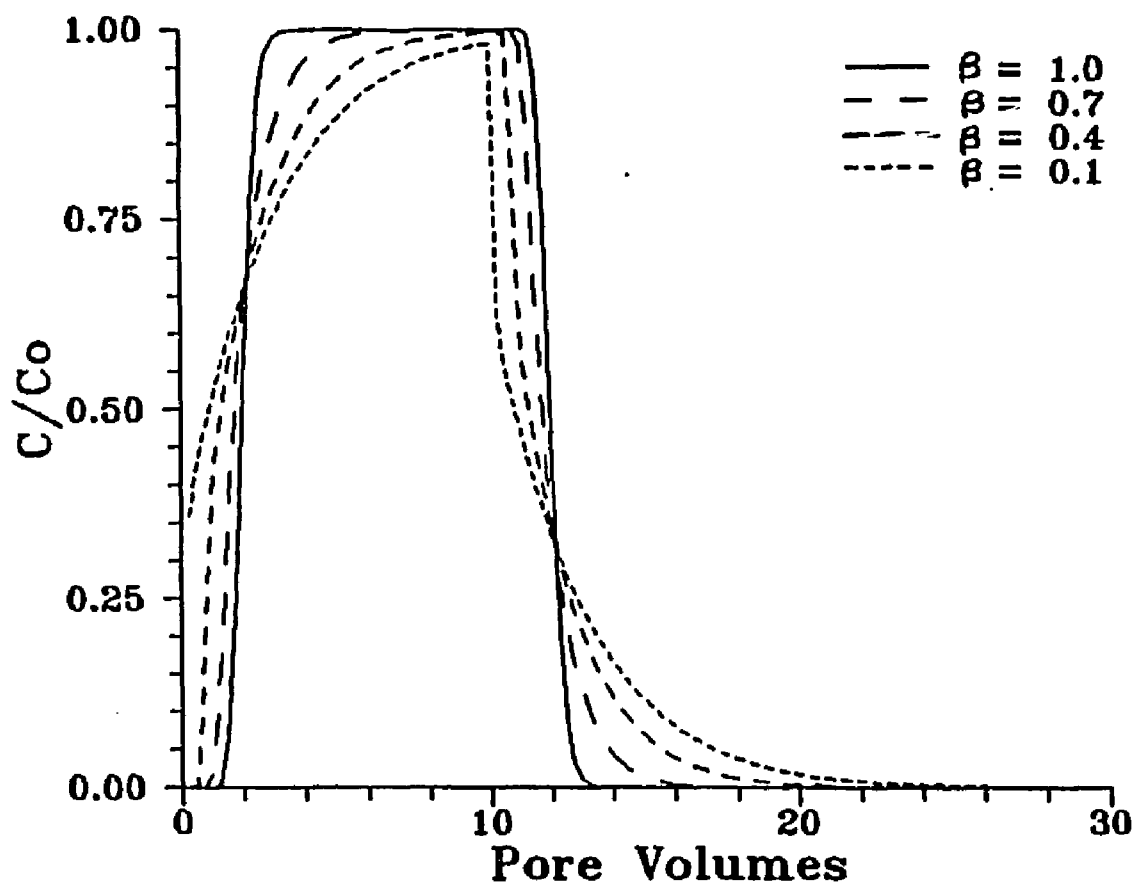


Figure 2.2.4. Effect of β on the breakthrough curve. Breakthrough curves represent two-compartment systems with $R = 2$, $P = 60$, $T_1 = 10$, and $\omega = 1.0$ (see following text for definition of ω).

$$\omega = \alpha_v \frac{L}{v_a} (R-1) \quad (2.2.18)$$

where the expressions for R and β are those that correspond to the given model.

If the micro-scale processes are fast relative to the rate of advection, ω will increase. Slow chemical processes have larger time scales and therefore result in a smaller ω . This results in greater tailing of the breakthrough curve at low values of ω (Figure 2.2.5). Schwarzenbach and Westall (1981) report that ω values greater than 50 occur in systems at equilibrium, while smaller values for ω imply that the system is subject to a slow chemical process.

2.3 Non-linear Least Squares Curve-fitting using CFITIM

The curve-fitting program, CFITIM, of van Genuchten (1981) contains subroutines which fit breakthrough curves to the analytical solutions of the mathematical models presented in the previous section. The program uses non-linear least-squares regression to determine estimates for the values of the dimensionless parameters.

The difference between the simulated and input data is quantified by the sum of the squared error (SSQ) value given in the program output file. The optimum values for the fitting parameters are listed in the program output file. The 95 percent confidence interval for each fitted parameter is given in the output. The fitted parameters can then be used to determine dispersion (using the value of P in Eqn. 2.2.11), the soil-water partition coefficient (using the value of R in Eqn. 2.2.9 or 2.2.10, depending on the model used), the fraction of mass

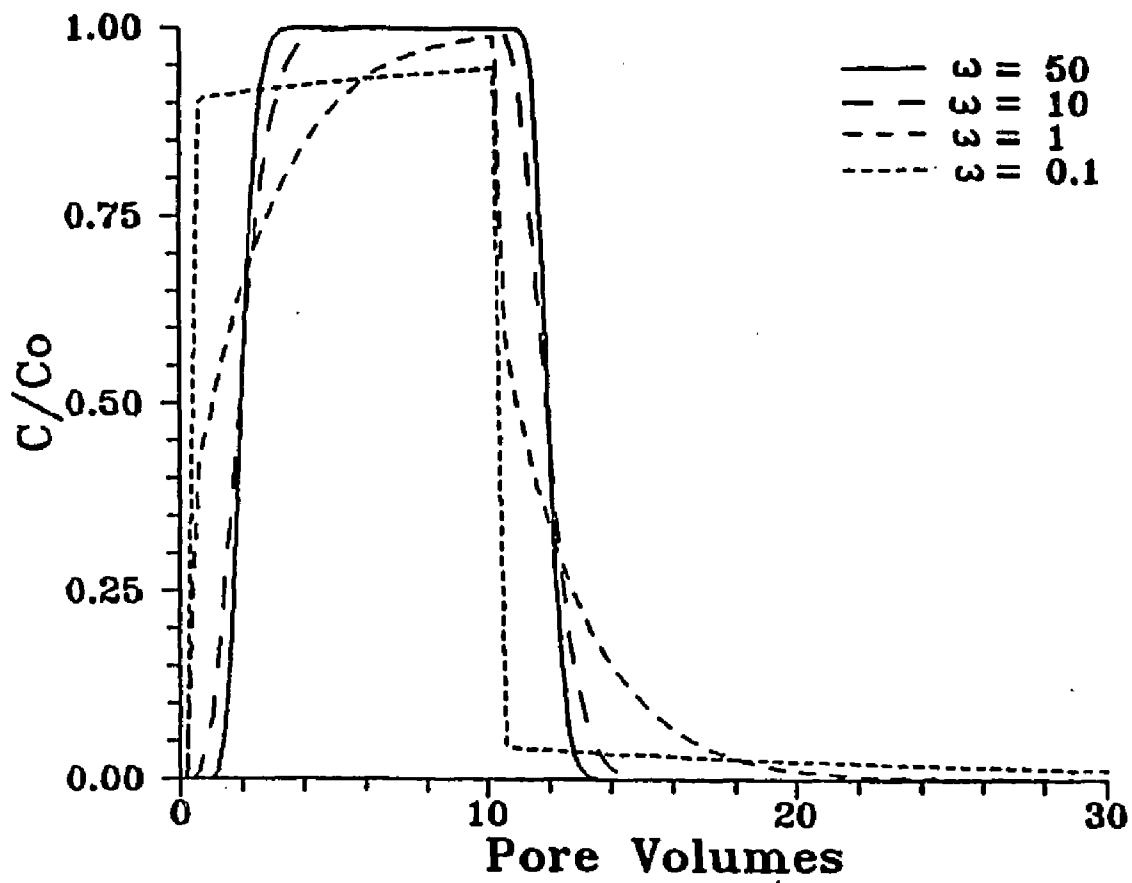


Figure 2.2.5. Effect of ω on the breakthrough curve. Breakthrough curves represent two-compartment systems with $R = 2$, $P = 70$, $T_1 = 10$, and $\beta = 0.2$.

sorbed to fast sites (using the value of β in Eqn. 2.2.15), and coefficients related to non-equilibrium processes (using the value of ω in Eqns. 2.2.16, 2.2.17, or 2.2.18, depending on the model used).

The equilibrium model contains three parameters (P , R , and T_1), the one-site kinetic and slow diffusion models contain four parameters (P , R , T_1 , and ω), and the two-compartment model has five parameters (P , R , T_1 , ω , and β).

CHAPTER 3

MATERIALS AND METHODS

3.1 Chemicals

The chemicals used for this study were HPLC grade and were purchased from Aldrich Chemical Company, Inc., Milwaukee, Wisconsin. After testing for impurities, the chemicals were used as received.

3.2 Soil

Soil used for this study was excavated during the removal of an underground storage tank in Phoenix, Arizona. It was taken from a depth of 0 to 17 feet. A test for VOCs indicated that there were no detectable levels. Gravitric measurements performed in the laboratory on cores taken from the field site showed the moisture content of the site to be 15 percent and the bulk density to be 1.5 g/cm³. These cores were disturbed during transportation from the field site so these values are approximations. f_{oc} was determined by a local laboratory using the phosphoric acid digestion and combustion method. The average value of four separate measurements was found to be 0.00097 ± 0.00014 grams organic carbon/gram soil.

3.2.1 Sample Preparation

The soil was oven dried at 105°C for 24 hours and was found to contain aggregates. The soil was then dry sieved for 20 minutes. Other than sieving, no effort was made to break up the aggregates. In order to deactivate any micro-

organisms that could degrade the compounds, the soil was autoclaved for 30 minutes at a temperature of 120°C and a pressure of 15 psig. The soil was then covered and stored in an oven at 105°C until use.

3.2.2 Preparation of Soil Columns

Before packing the columns, the gravel fraction of the soil was removed in order to reduce scale problems. The silt and clay fractions were removed because they caused an increase in pressure when air was passed through the column that could not be sustained by the column fittings. The soil was then mixed in order to ensure uniformity.

The columns, which were 30 cm in length and 2.7 cm in diameter, were oriented vertically and packed by pouring approximately 30 grams of soil into the column, stirring the soil to remove any stratification, and tamping in a circular pattern to achieve a uniform bulk density. This procedure was repeated until the column was filled with soil.

Fiberglass 'wool' was placed at the inflow end to enhance the uniformity of the flow field. The column was then sealed with teflon tape and fittings. A 10 μm mesh teflon screen was inserted into the downstream column fitting to impede movement of any fine-grained particles out of the column.

The desired moisture content was attained by siphoning a predetermined volume of water into the column. The siphon was created by placing a graduated cylinder containing the desired amount of water above the top of the column and

a vacuum at the bottom. The column was used only after it appeared that the soil water was uniformly distributed.

For this study, soil columns of two different moisture contents were used. The dry column had a moisture content of 9 percent, an air-filled porosity of 28 percent, a total porosity of 37 percent, and a bulk density of 1.67 g/cm^3 . There were two wet columns prepared. The first wet column had a moisture content of 18 percent, an air-filled porosity of 18 percent, a total porosity of 36 percent, and a bulk density of 1.70 g/cm^3 . This column was used for the benzene soil venting experiments. The second wet column had a moisture content of 18 percent, an air-filled porosity of 17 percent, a total porosity of 35 percent, and a bulk density of 1.72 g/cm^3 . This column was used for the *p*-xylene soil venting experiments, the helium tracer experiments, and the flow versus pressure experiments. The consistency of the bulk density, air-filled porosity, and total porosity values indicates that the packing and wetting procedure used gives reproducible results.

3.3 Helium Tracer Experiments

The helium tracer experiments were conducted to determine the contribution of dispersion and diffusion to the transport of VOC in the unsaturated zone during forced ventilation. Helium was used as a conservative tracer because it does not sorb to soil and is sparingly soluble ($0.0094 \text{ cm}^3 \text{ He/cm}^3 \text{ water}$, CRC, 1981). Additionally, breakthrough curves obtained from these experiments were used to calibrate the flow meter.

3.3.1 Apparatus

The apparatus used for the helium tracer experiments is shown in Figure 3.3.1 and consisted of: (1) a pressurized cylinder of air with pressure regulator to induce flow through the system, (2) a flow control valve, (3) three gas washing bottles containing water to keep the air flowing into the column saturated, (4) a syringe pump containing a 10-ml gas-tight syringe to inject helium into the system, (5) a Matheson flow meter (model 610A), (6) a U-tube mercury manometer to measure pressure, (7) the soil column (kept at a constant temperature of 22.5°C by means of a water jacket connected to a constant temperature water bath), and (8) a Gow Mac gas leak detector (model 21-150) which was used to measure the helium concentration as a function of time.

3.3.2 Experimental Procedure

The steps involved in the helium tracer experiments were: (1) zeroing the gas leak detector with respect to clean air, (2) achieving a steady input helium concentration large enough to cause a 60 percent deflection on the gas leak detector using the syringe pump/syringe assembly, (3) loading the soil column with helium and recording the increase in concentration as a function of time, and (4) disconnecting the syringe pump/syringe assembly and allowing clean air to remove the helium from the column and recording the decrease in concentration as a function of time. The concentration versus time data yielded breakthrough curves which were analyzed to obtain estimates for dispersion coefficients. The four basic steps are discussed in greater detail below.

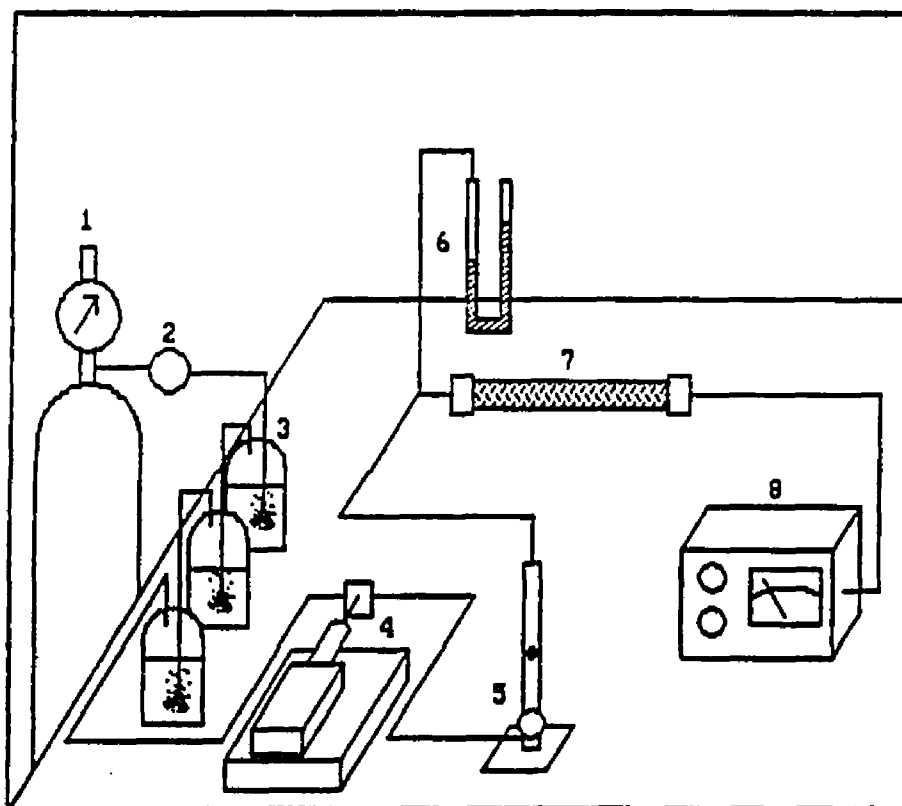


Figure 3.3.1. Experimental apparatus used for helium tracer and flow vs. pressure experiments. Components are: 1. pressure cylinder equipped with pressure regulator, 2. flow control valve, 3. gas washing bottles containing water, 4. syringe pump, 5. flow meter, 6. manometer, 7. soil column, and 8. gas leak detector.

When beginning a helium tracer experiment, clean air was allowed to flow through the soil column until a steady flow rate was obtained. The flow was then allowed to equilibrate for approximately five minutes. This initial equilibration period was found to be adequate to ensure that the flow did not vary during an experiment. The gas leak detector was zeroed relative to the clean air flowing from the soil column. The syringe pump/syringe assembly was not present in the system for this step. Once a steady flow was attained, the soil column was disconnected, and the syringe pump/syringe assembly was introduced into the system. The injection rate of the syringe pump was set so that a deflection of the gas leak detector of at least 60 percent was obtained. Once this was accomplished, the soil column was reconnected, the detector probe was inserted in the outflow end of the soil column, and the experiment was started. Inserting (or removing) the syringe/syringe pump assembly resulted in no noticeable change in the flow rate.

The deflection of the gas leak detector (i.e., the relative helium concentration) was recorded as a function of time as the column was being loaded with helium. When the deflection of the gas leak detector was constant for a period of a few minutes, the syringe pump/syringe assembly was removed, and clean air was used to remove the helium from the column. The design of the apparatus did not allow for sampling of the inflow concentration; therefore, the steady-state deflection observed during loading was taken to be the inflow concentration.

Flow, pressure, and relative helium concentration were monitored throughout each experiment. The flow meter reading was recorded every time a gas leak

detector reading was recorded. The flow meter readings were then time averaged and converted to volumetric flow rates using the value for the gravimetric pore volume and the value of t_{res} .

A listing of the helium tracer experiments performed is given in Table

3.3.1. The data obtained from these experiments were reproducible.

3.3.3 Flow Meter Calibration

The deflection of the gas leak detector, when normalized by the maximum observed deflection and plotted as a function of dimensionless time (pore volumes), yields a breakthrough curve which has a normal distribution. Helium is assumed to be a conservative tracer (i.e., $R = 1$); thus, the sinuous shape of the breakthrough curve is caused entirely by the dispersive and diffusive properties of the porous medium and the diffusive properties of the tracer.

The normal distribution of the breakthrough curves coupled with the conservative nature of helium allows for the assumption that one pore volume breaks through at the time when the outflow concentration is one-half the inflow concentration (i.e., $C_1 = 0.50$). The time taken to achieve $C_1 = 0.50$ will be referred to as t_{50} . Due to the symmetry of the breakthrough curves, t_{50} is equivalent to t_{res} . Using the value of the gravimetrically-determined pore volume (ml) and normalizing it by t_{50} (min) gives the flow for a given experiment in ml/min. These flows were plotted as a function of the flow meter reading in order to generate calibration curves for each column. The results of the flow meter

Table 3.3.1 Listing of Helium Tracer Experiments

| Exp | θ_w (cm ³ _w /cm ³) ^a | θ_a (cm ³ _a /cm ³) ^b | Flow Meter Reading ^c |
|-------------------|---|---|------------------------------------|
| H1W | 0.18 | 0.17 | 17 |
| H2W | 0.18 | 0.17 | 27 |
| H3W | 0.18 | 0.17 | 38 |
| H4W | 0.18 | 0.17 | 47 |
| H5W | 0.18 | 0.17 | 57 |
| H3Wr ^d | 0.18 | 0.17 | 37 |
| H1D | 0.09 | 0.28 | 19 |
| H2D | 0.09 | 0.28 | 34 |
| H3D | 0.09 | 0.28 | 47 |
| H4D | 0.09 | 0.28 | 54 |
| H5D | 0.09 | 0.28 | 66 |
| H2Dr ^d | 0.09 | 0.28 | 36 |

^a cm³ water/cm³ total (porous media).

^b cm³ air/cm³ total (porous media).

^c Flow meter readings represent time-averaged readings.

^d Reproduced experiments.

calibration are given in Table 3.3.2. The calibration curves for both columns are shown in Figure 3.3.2.

Best-fit power functions to the data were as follows:

$$\text{Wet column} \quad Q = 0.12M^{1.25} \quad (3.3.1)$$

$$\text{Dry column} \quad Q = 0.11M^{1.38} \quad (3.3.2)$$

where Q is the flow in ml/min and M is the flow meter reading.

Figure 3.3.2 indicates that the dry column gave consistently higher flows for a given flow meter reading than the wet column. This difference may be the result of assuming the gravimetric pore volume to be equivalent to the effective pore volume when calculating flow. The effective pore volume is usually less than the gravimetric pore volume since some pores are disconnected from the conductive (effective) pores.

A t -test showed that the 95 percent confidence interval of the exponents of the two calibration curves do not overlap. Therefore, separate calibration curves are used for the wet and dry soil columns.

Calibration curve data for the wet column were reproducible over the entire range of flows used except for the highest flow rate. Reproduced flows in the high range tend to be higher than those predicted by the calibration curve indicating a change in pore geometry due to the high pressure gradients involved. A fracture in the soil column will have the same effect; however, there was no

Table 3.3.2 Flow Meter Calibration Curve Data

| Exp | t_{50} (min) | Q (ml/min) | Flow Meter Reading |
|------------------|-------------------|---------------|-----------------------|
| H1W ^a | 7.45 | 3.97 | 17 |
| H2W ^a | 3.94 | 7.51 | 27 |
| H3W ^a | 2.85 | 10.39 | 38 |
| H4W ^a | 2.24 | 13.21 | 47 |
| H5W ^a | 1.53 | 19.35 | 57 |
| H1D ^b | 7.26 | 6.46 | 19 |
| H2D ^b | 3.92 | 11.96 | 34 |
| H3D ^b | 2.55 | 18.39 | 47 |
| H4D ^b | 1.99 | 23.57 | 54 |
| H5D ^b | 1.25 | 37.52 | 66 |

^a Gravimetric pore volume = 29.6 ml

^b Gravimetric pore volume = 46.9 ml

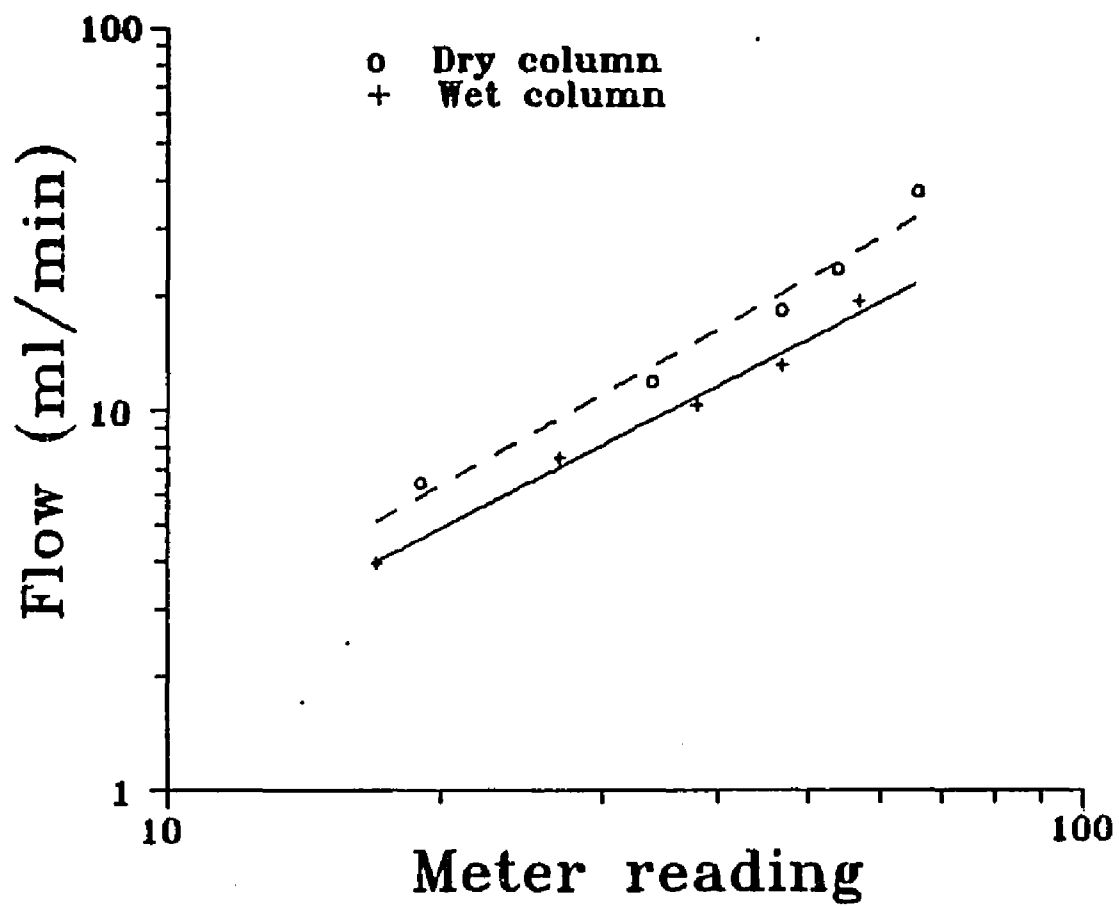


Figure 3.3.2. Flow meter calibration curves for the wet and dry soil columns.

drop in pressure indicating that the column was not fractured. Calibration curve data for the dry column were reproducible over the entire range of flows used.

3.4 Flow versus Pressure Experiments

The flow versus pressure experiments were conducted in order to determine the air permeability of the soil columns and whether flow was compressible or incompressible at the pressures used for the soil venting experiments.

For advective vapor phase flow through porous media, compressibility of the gas should be considered when calculating the Darcy velocity. Eqn. 3.4.1 (Kilbury et al., 1986) describes the flow of air through porous media and accounts for contributions to flow due to compression.

$$q_v = - k_a(dp/dx)/\mu - k_a(dp^2/dx)/(2\mu p_o) \quad (3.4.1)$$

where k_a = air permeability (cm^2); dp/dx = pressure gradient (atm/cm); p_o = reference pressure (atm); and μ = dynamic viscosity of air at 22.5°C (1.80×10^{-10} atm sec , interpolated value from Roberson and Crowe, 1985).

If flow is incompressible, the second (non-linear) term can be ignored, and Eqn. 3.4.1 reduces to a linear equation which is Darcy's Law in rectangular coordinates (Hillel, 1980):

$$q_v = - (k_a/\mu)(dp/dx) \quad (3.4.2)$$

3.4.1 Apparatus

The apparatus used for the flow versus pressure experiments was identical to that used for the helium tracer experiments (Figure 3.3.1).

3.4.2 Experimental Procedure

The experimental procedure used for the flow versus pressure experiments was identical to that used for the helium tracer experiments with the exception that all valves upstream of the soil column and downstream of the manometer were fully opened. This was done to ensure that the deflection in the manometer (i.e., the recorded pressure) was due to the soil column. The pressure drop across the column (dp) for a given flow (q_v) was recorded. These data were used to determine k_a (using Eqns. 3.4.1 and 3.4.2) and whether flow was compressible (using Eqn. 3.4.1).

The flow versus pressure experiments were run separately from the helium tracer experiments. Helium was used during these experiments to confirm the results of the flow meter calibration curve. A listing of the flow versus pressure experiments performed is given in Table 3.4.1.

3.4.3 Air Permeability Studies

The calculation of the air permeability of a soil column requires the measurement of the pressure gradient across the column and the resultant flow expressed as the Darcy velocity (q_v).

Table 3.4.1 Listing of Flow versus Pressure Experiments

| Exp | q_v (cm/sec) | dp^a (atm) |
|-------------------|-------------------|-----------------|
| Wet soil column | | |
| P1W | 0.014 | 0.018 |
| P2W | 0.029 | 0.055 |
| P3W | 0.045 | 0.108 |
| P4W | 0.055 | 0.138 |
| P5W | 0.076 | 0.190 |
| P1Wr ^b | 0.012 | 0.013 |
| P2Wr ^b | 0.029 | 0.049 |
| P3Wr ^b | 0.042 | 0.100 |
| P4Wr ^b | 0.054 | 0.117 |
| P5Wr ^b | 0.069 | 0.159 |
| Dry soil column | | |
| P1D | 0.016 | 0.005 |
| P2D | 0.038 | 0.018 |
| P3D | 0.053 | 0.029 |
| P4D | 0.077 | 0.055 |
| P5D | 0.098 | 0.083 |
| P1Dr ^b | 0.016 | 0.003 |
| P2Dr ^b | 0.038 | 0.016 |
| P3Dr ^b | 0.051 | 0.026 |
| P4Dr ^b | 0.074 | 0.049 |
| P5Dr ^b | 0.096 | 0.075 |

^a Pressure was calculated as the product of the specific weight of mercury and the deflection of the manometer.

^b Reproduced experiments.

The calculated flows were in close agreement with those predicted by the calibration curves except for the highest velocity experiment using the wet column. In this experiment, the predicted q_v was 0.36 cm/sec, and the observed q_v , using the helium tracer breakthrough curve and gravimetric pore volume, was 0.53 cm/sec. This may be the result of a change in the pore geometry caused by the high pressure imposed on the column.

The q_v versus pressure data for both columns (Figure 3.4.1) show flow through the dry column to be greater for a given pressure than the wet column indicating that the dry column is more conducive to the flow of air (i.e., has a greater air permeability).

From q_v and dp , the value for k_a can be calculated by rearranging the flow models (Eqns. 3.4.1 and 3.4.2) and solving for k_a . Using the compressible flow model (Eqn. 3.4.1), the k_a values for the wet and dry columns were 0.21 darcy and 0.70 darcy, respectively. Using the incompressible flow model (Eqn. 3.4.2), the k_a values for the wet and dry columns were 0.22 darcy and 0.72 darcy, respectively. The difference in k_a values obtained using the two models is negligible. These values are within the limits proposed by Freeze and Cherry (1979) for a silty sand (0.01-100 darcy) and are on the low end of the range due to the presence of water.

3.4.4 Compressible Flow Studies

The q_v versus pressure data are linear for the wet column ($r^2 = 0.997$) as well as the dry column ($r^2 = 0.973$) indicating that vapor flow for both columns at

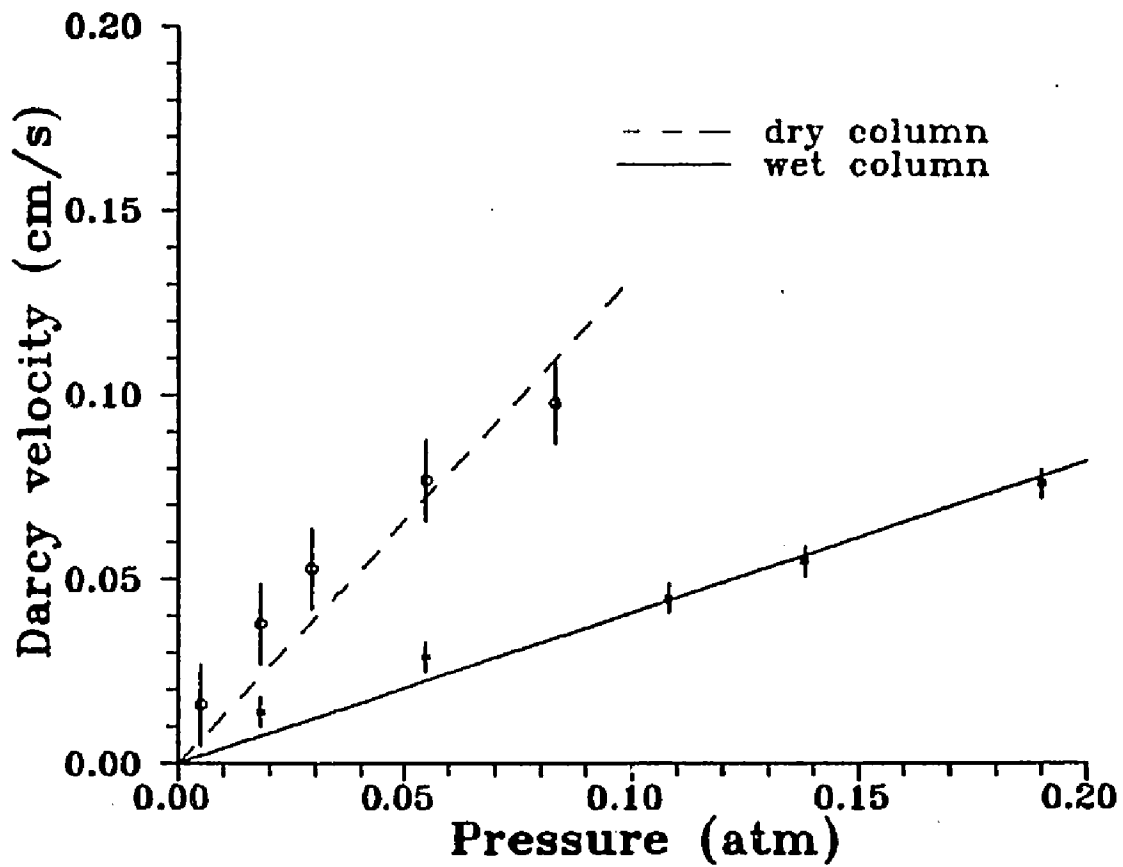


Figure 3.4.1. Darcy velocity vs. pressure. The error bars represent the standard error of estimate of a linear regression model forced through the origin.

the pressures used was incompressible. To determine the contribution of compressible flow effects due to the increased density resulting from the increase in pressure, the ratio of $dp^2/2p_0$ to dp was calculated. (The value of p_0 was taken to be the pressure at 2500 feet, the approximate elevation of Tucson). This ratio represents the independent variables involved after factoring the constants of Eqn. 3.4.1 and is interpreted as the fraction of flow resulting from compression and the subsequent increase in density to the total flow. This ratio increases as velocity increases indicating that at higher pressures, compressible effects take on increased importance. For the dry column, it was found that compression of the vapor accounted for 4 percent of the measured q_v at the highest velocity. For the wet column, compression of the vapor accounted for 9 percent of the measured q_v at the highest velocity. These percentages were determined to be insignificant.

3.5 Soil Venting Experiments

The soil venting experiments were conducted in order to determine the important rate-limiting processes during the removal of VOCs (benzene and *p*-xylene) from the vadose zone using forced ventilation. Moisture content, initial level of concentration, and vapor velocity were varied in order to determine the effect these parameters had on removal.

The experimental procedure and results of the soil venting experiments are described in more detail in Davis (1989). The following is a brief description of the apparatus and experimental procedure.

3.5.1 Apparatus

The apparatus used for the soil venting experiments is similar to the apparatus used for the helium tracer and flow versus pressure experiments and is shown in Figure 3.5.1. The apparatus consisted of: (1) a pressurized cylinder of air with pressure regulator to induce flow through the system, (2) a flow control valve, (3) two gas washing bottles containing water to keep the inflowing air saturated, (4) directional flow valves used to route flow through a gas washing bottle containing the VOC, (5) when loading the soil column or through a third gas washing bottle containing water, (6) when stripping the compound from the soil column, (7) a flow control valve used to alter the input concentration, (8) the flow control valve, (9) an upstream sampling port used to monitor inflow concentration, (10) a U-tube mercury manometer to measure pressure, (11) the soil column, which was kept at a constant temperature of 22.5°C by means of a water jacket connected to a constant temperature water bath, (12) a downstream sampling port used to monitor outflow concentration, and (13) a suspended bead flow meter to measure flow.

All components downstream of the gas washing bottle containing the VOC were made of teflon, stainless steel, or glass to minimize sorption onto the apparatus.

3.5.2 Experimental Procedure

The steps used for the soil venting experiments were: (1) attaining a steady flow rate and constant input concentration, (2) loading the column with the VOC,

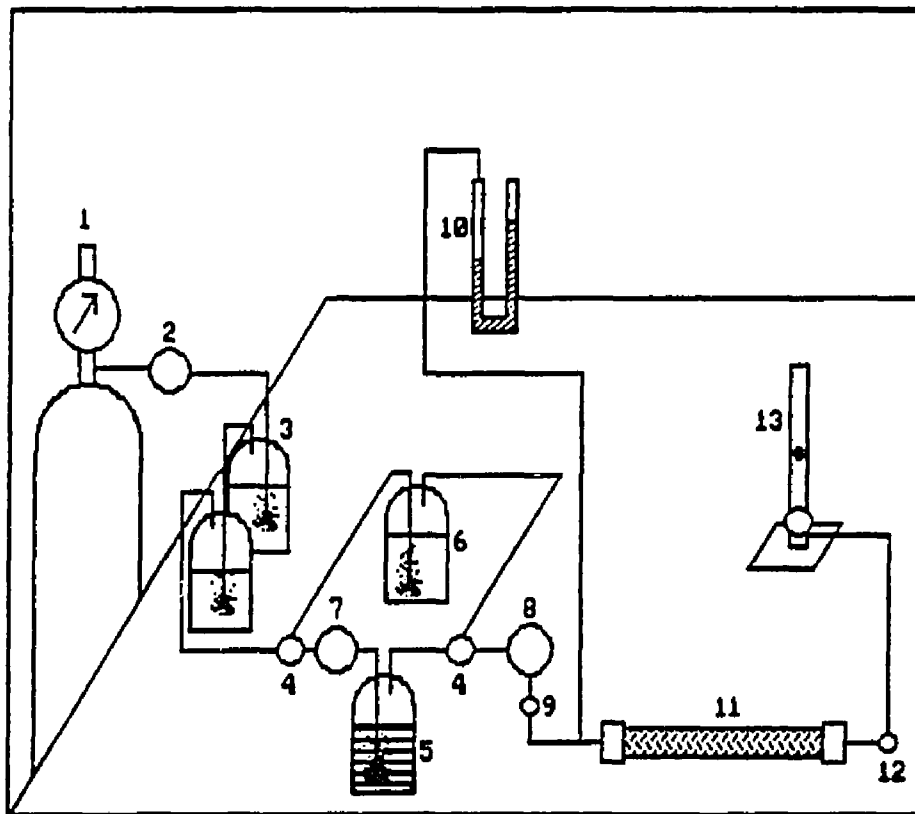


Figure 3.5.1. Experimental apparatus used for soil venting experiments. Components are: 1. pressure cylinder equipped with pressure regulator, 2. flow control valve, 3. gas washing bottles containing water, 4. directional flow valves, 5. gas washing bottle containing VOC, 6. gas washing bottle containing water, 7. flow control valve, 8. flow control valve, 9. sampling port, 10. manometer, 11. soil column, 12. sampling port, 13. flow meter.

(3) sampling the inflow and outflow concentrations and recording the time at which samples were taken, and (4) removing the VOC from the column and sampling the outflow concentration and the recording the time at which samples were taken.

Before introducing the VOC into the soil column, the flow and input concentration was steadied. Samples were drawn from the apparatus through teflon-lined septa sampling ports using a 100- μ l gas-tight syringe. The samples were then injected into a Varian 3700 gas chromatograph equipped with a flame ionization detector (FID). The output of the detector was analyzed using a Hewlett-Packard 3390A integrator. The gas chromatograph was calibrated with standards before and after each soil venting experiment to ensure equipment consistency and data quality (Davis, 1989). The calibration curves for the gas chromatograph were linear over the range of concentrations used. Input concentration was varied by splitting the flow and using a flow control valve to control the amount of flow routed through the VOC bottle. The remaining flow was routed around the VOC bottle and through an additional gas washing bottle containing water. The clean and contaminated air was recombined down-stream of the VOC bottle and upstream of the inflow sampling port.

The time at which each sample was taken was recorded. While loading the column with the VOC, the inflow and outflow concentrations were monitored. The input concentration was erratic due to variations in flow and as a result, the outflow concentrations during loading were also erratic. When the outflow concentration matched the inflow concentration for a time period of approxi-

mately 30 minutes, clean air was introduced into the column to remove the VOC. In order to prevent any additional VOC from entering the soil column via diffusion, the VOC bottle was removed from the system. As before, the outflow concentration was monitored as a function of time.

Flow was monitored and adjusted as necessary using the valve immediately upstream of the inflow sampling port. The flow meter reading was recorded every time a sample was taken. The flow meter readings were then time averaged and converted to a volumetric flow using the calibration curves developed from the helium tracer experiments.

The moisture content was determined gravimetrically before and after each experiment. The moisture content for both the wet and dry columns remained constant for all experiments performed.

The room temperature was also monitored, and changes of 4°C (relative to the column temperature) were observed for some experiments. The sampling port was outside the temperature jacket and was therefore not temperature controlled. The distance between the exit point (temperature controlled) and sampling point (not temperature controlled) was on the order of millimeters.

Pressure was also monitored during the experiments. The pressure was constant indicating there were no changes in pore geometry during the experiments.

A listing of all soil venting experiments performed is given in Table 3.5.1.

Table 3.5.1 Listing of Soil Venting Experiments

| Exp | θ_w (cm ³ _w /cm ³) ^a | θ_a (cm ³ _a /cm ³) ^b | v_a^c (cm/sec) | C_o (mg/l) |
|------------------------|---|---|---------------------|-----------------|
| Benzene | | | | |
| B3 | 0.18 | 0.18 | 0.19 | 348 |
| B4 | 0.18 | 0.18 | 0.19 | 374 |
| B5 | 0.18 | 0.18 | 0.30 | 426 |
| B6 | 0.18 | 0.18 | 0.10 | 389 |
| B8 | 0.18 | 0.18 | 0.10 | 149 |
| B9 | 0.18 | 0.18 | 0.29 | 152 |
| B10 | 0.18 | 0.18 | 0.19 | 105 |
| B15 | 0.09 | 0.28 | 0.13 | 357 |
| B16 | 0.09 | 0.28 | 0.23 | 368 |
| B17 | 0.09 | 0.28 | 0.33 | 344 |
| <i>p</i>-xylene | | | | |
| XY1 | 0.09 | 0.28 | 0.32 | 35 |
| XY2 | 0.09 | 0.28 | 0.33 | 45 |
| XY3 | 0.09 | 0.28 | 0.14 | 35 |
| XY4 | 0.09 | 0.28 | 0.21 | 32 |
| XY5 | 0.18 | 0.17 | 0.10 | 37 |
| XY6 | 0.18 | 0.17 | 0.19 | 33 |
| XY7 | 0.18 | 0.17 | 0.30 | 34 |
| XY8 | 0.18 | 0.17 | 0.19 | 16 |
| XY9 | 0.18 | 0.17 | 0.30 | 15 |
| XY10 | 0.18 | 0.17 | 0.11 | 13 |

^a cm³ water/cm³ total (porous media).

^b cm³ air/cm³ total (porous media).

^c Obtained using the corresponding calibration curve for the column used.

3.6 Saturated Column Experiments

A series of three saturated column experiments were performed in order to obtain independent estimates of kinetic rate coefficients, kinetic time scales, and K_p for benzene. No saturated column experiments were performed using *p*-xylene.

The apparatus and procedure were similar to that used in the soil venting experiments. The only major difference was that a constant pressure pump was used to move benzene in an aqueous phase solution through the soil column.

Mass balance problems occurred, and erratic data were obtained as the result of a faulty feed system which consisted of a teflon bag containing the VOC solution upstream of the pump. The problem with the feed system was that benzene vapors diffused through the teflon bag resulting in inflow concentrations that decreased with time. As a result, the results of only one of the three saturated experiments will be presented (experiment SAT2). The experimental parameters for experiment SAT2 were as follows: $Q = 0.76$ pore volumes/hour, velocity = 0.003 cm/sec, input volume = 3.81 pore volumes. The porosity of the column used was 37 percent; the bulk density = 1.67 g/cm³. One pore volume was 29.8 cm³.

CHAPTER 4

RESULTS

4.1 Helium Tracer Experiments

The helium tracer experiments were used to determine the mechanical dispersion of the partially-saturated soil columns and its relation, if any, to velocity. Breakthrough curves were analyzed using the non-linear least squares curve-fitting program, CFITIM (van Genuchten, 1981). Dispersion was estimated using the equilibrium model because of the symmetry displayed in the breakthrough curves (Figure 4.1.1). Fits were good with the sum of the squared errors (SSQs) ranging from 0.002 to 0.023. Experiment H3W, shown in Figure 4.1.1, is representative of the ten experiments; the remaining breakthrough curves are contained in Appendix A.

Fitted retardation (R) factors were within 11 percent of the calculated value of 1.0. Fitted values of pulse (T_p) were also in close agreement with the measured values (based on flow meter readings and time measurements), thus confirming mass balance. Dimensionless parameters estimated by the curve-fitting program are listed in Table 4.1.1.

Dispersion (D) is specific to the porous media as well as the contaminant being transported. For purposes of this study, it is assumed that dispersion results from two processes: (1) pore scale velocity variations, and (2) molecular diffusion; both of which cause a broadening of the solute front.

The first process is called mechanical dispersion (D_m) which is assumed to be constant for the porous media at a given moisture content and shows the same

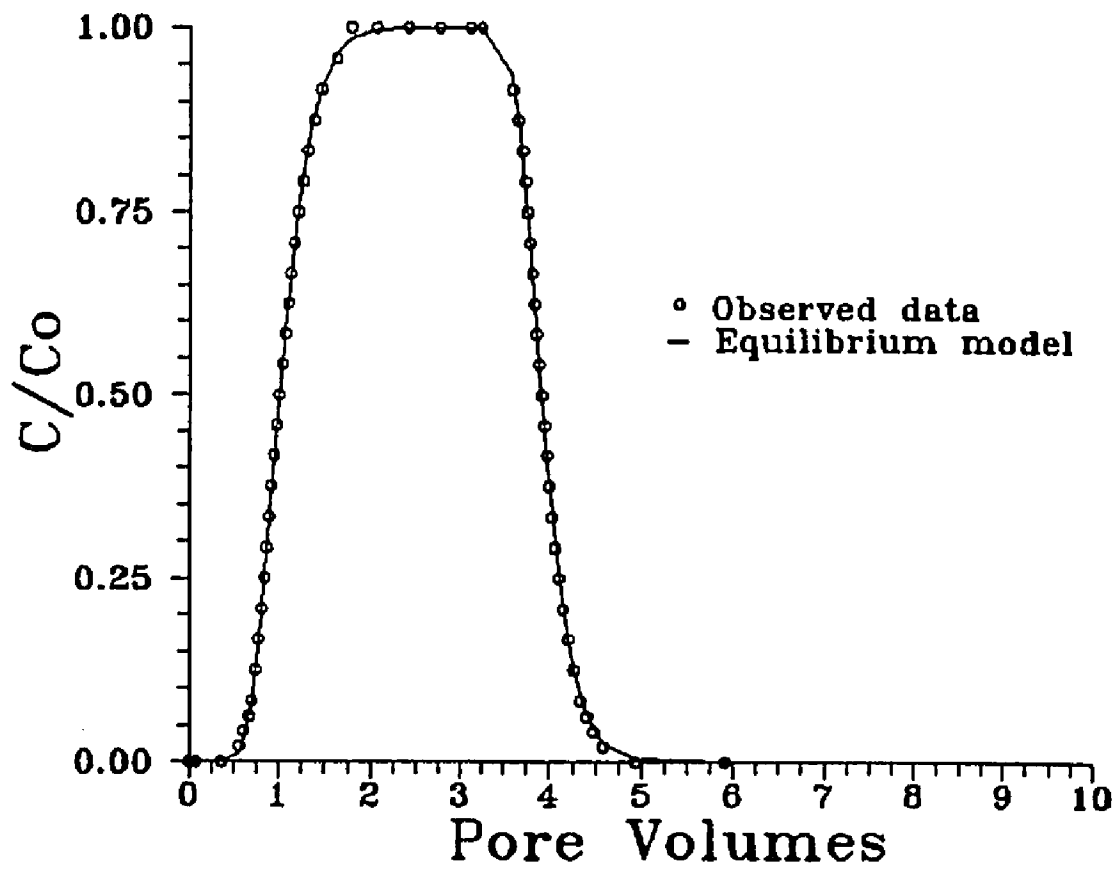


Figure 4.1.1. Observed and fitted data for experiment H3W using the equilibrium model.

Table 4.1.1 Curve-fitting Results for the Helium Tracer Breakthrough Curve Data using the Equilibrium Model^a

| Exp | v_a (cm/sec) | SSQ | P | R^b | T_1^b |
|-----------------|-------------------|-------|------|------------|-----------|
| Wet soil column | | | | | |
| H1W | 0.07 | 0.008 | 16.2 | 1.06 (1.0) | 2.6 (2.6) |
| H2W | 0.13 | 0.002 | 26.4 | 1.04 (1.0) | 2.9 (3.1) |
| H3W | 0.18 | 0.002 | 27.8 | 1.04 (1.0) | 2.9 (3.2) |
| H4W | 0.23 | 0.023 | 31.3 | 1.04 (1.0) | 3.2 (3.6) |
| H5W | 0.33 | 0.018 | 33.2 | 1.04 (1.0) | 3.5 (3.9) |
| Dry soil column | | | | | |
| H1D | 0.07 | 0.012 | 8.1 | 1.11 (1.0) | 2.9 (2.9) |
| H2D | 0.12 | 0.002 | 15.9 | 1.06 (1.0) | 3.5 (3.6) |
| H3D | 0.19 | 0.002 | 28.8 | 1.03 (1.0) | 3.0 (3.2) |
| H4D | 0.24 | 0.003 | 37.3 | 1.02 (1.0) | 2.8 (3.0) |
| H5D | 0.39 | 0.017 | 54.5 | 1.01 (1.0) | 2.5 (2.8) |

^a An absolute value of C_0 could not be determined from the gas leak detector.

^b Measured values are given in parentheses.

mathematical behavior as the molecular diffusion coefficient (D_o) appearing in the diffusion equation (Fischer et al., 1979). Therefore, unlike slow processes, mechanical dispersion does not affect the symmetry of the breakthrough curve.

Porous media diffusion (D_d) is a property of the pore geometry as well as the compound. Many different expressions for D_d/D_o are contained in the literature. A partial listing of porous media diffusion models appearing in the literature is given in Table 4.1.2. The expression proposed by Lai et al. (1976) was chosen because it gave mid-range D_d/D_o values (Figure 4.1.2) based on the characteristics of the columns used when compared to other models.

D_o is the molecular diffusion coefficient for species 'B' diffusing through species 'A' or vice versa. The value of D_o is calculated using the Chapman-Enskog kinetic theory of gaseous diffusion (Welty et al., 1976):

$$D_o = (0.001858)T^{3/2}(1/M_A + 1/M_B)^{1/2}/(p\sigma_{AB}^2\Omega) \quad (4.1.1)$$

where D_o = molecular diffusion coefficient (cm^2/sec), T = absolute temperature (K), M_A = molecular weight of molecule A (g), M_B = molecular weight of molecule B (g), p = pressure (atm), σ_{AB} = collision diameter (Å), and Ω = collision integral (dimensionless).

The underlying assumptions of this equation are: (1) the system consists of only two gases, (2) the gas molecules are non-polar (there is no transport due to electrostatic attraction), and (3) the system has a low density (there is no transport due to gravity flow). A third component, water vapor, was initially considered

Table 4.1.2 Porous Media Vapor Diffusion Models

| Model | D_d/D_o | Reference |
|-------|----------------------------|--------------------------------|
| 1 | $0.31-0.59e_w$ | de Jong and Schappert (1972) |
| 2 | $0.777e_s/(e_s+e_w)-0.274$ | Albertson (1979) |
| 3 | $0.66e_s$ | Penman (1940) |
| 4 | $0.61e_s$ | van Bavel (1951) |
| 5 | $e_s^{4/3}$ | Lai et al. (1976) ^a |
| 6 | $e_s^{3/2}$ | Marshall (1959) |
| 7 | $5.25e_s^{2.38}$ | Grable and Siemer (1968) |
| 8 | $0.9e_s-0.1$ | Wesseling (1962) |
| 9 | $e_s^{10/3}/(e_s+e_w)^2$ | Millington (1959) |
| 10 | $e_s^4/(e_s+e_w)^{7/2}$ | Currie (1970) |

^a Model used for this study.

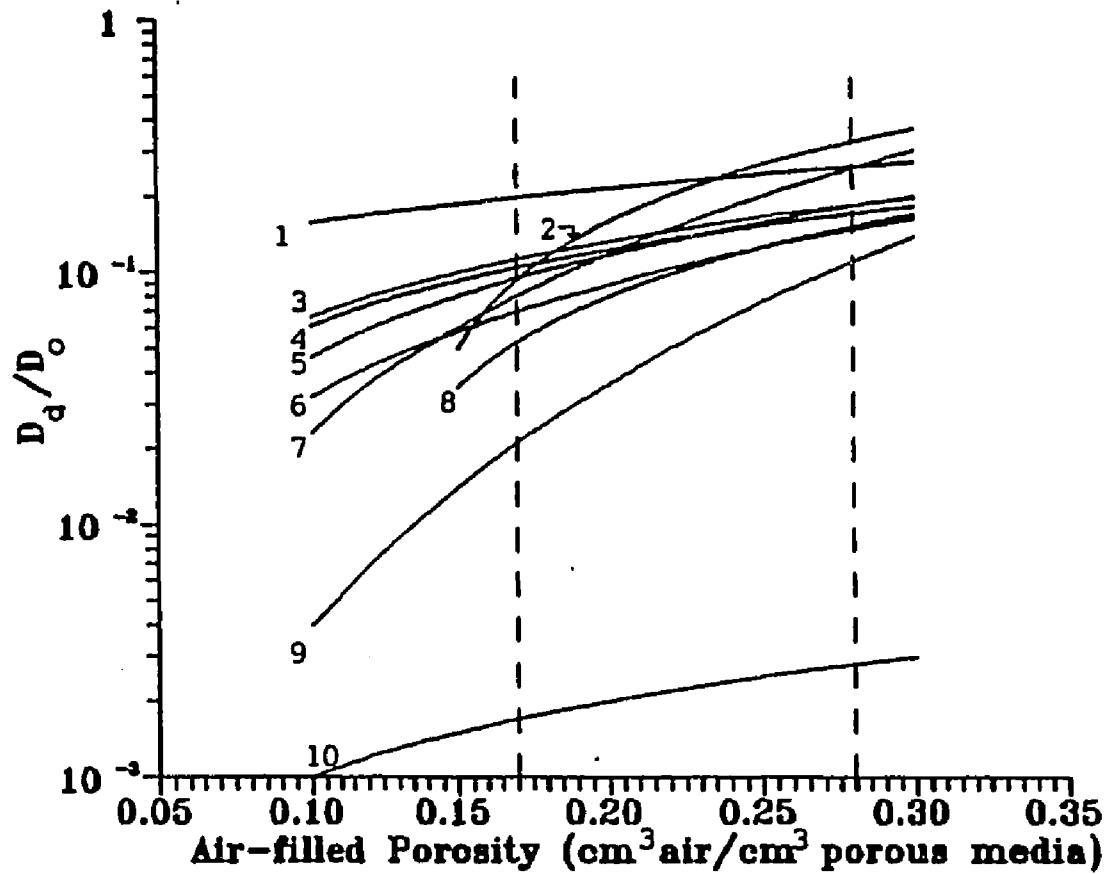


Figure 4.1.2. D_d/D_o vs. θ_a based on porous media diffusion models appearing in the literature. Numbers correspond to the models given in Table 4.1.2. The vertical dashed lines show the range of θ_a used for this study.

in the calculations and was found to have no effect. Calculated D_o values were as follows: D_o for helium = 0.76 cm²/sec, D_o for benzene = 0.09 cm²/sec, and D_o for *p*-xylene = 0.07 cm²/sec.

Like mechanical dispersion, porous media diffusion results in a broadening of the breakthrough curve. Since these two processes have a similar effect on transport, (although the mechanisms are different), they are summed to yield the hydrodynamic dispersion coefficient (D):

$$D = D_m + D_d \quad (4.1.2)$$

where D_m and D_d are expressed in units of cm²/sec.

Dispersion (D) is calculated from P given v_a and L ($D = v_a L/P$). Mechanical dispersion (D_m) is calculated from D by substituting the porous media diffusion values (D_d) determined using the model of Lai et al. (1976). The values of D_m for each velocity are listed in Table 4.1.3.

Best-fit power functions relating D_m and v_a indicate that mechanical dispersion is directly related to velocity in the wet column and is independent of velocity in the dry column (Figure 4.1.3). The best-fit curves are:

$$\text{Wet Column} \quad D_m = 0.88v_a^{1.32} \quad (4.1.3)$$

$$\text{Dry Column} \quad D_m = 0.04v_a^{-0.41} \quad (4.1.4)$$

Table 4.1.3 Dispersion, Mechanical Dispersion, and Porous Media Diffusion for the Wet and Dry Soil Columns

| v_a (cm/sec) | D (cm ² /sec) | D _d (cm ² /sec) | D _m (cm ² /sec) |
|-------------------|-----------------------------|--|--|
| Wet soil column | | | |
| 0.07 | 0.13 | 0.10 | 0.03 |
| 0.13 | 0.15 | 0.10 | 0.05 |
| 0.18 | 0.19 | 0.10 | 0.09 |
| 0.23 | 0.22 | 0.10 | 0.12 |
| 0.33 | 0.30 | 0.10 | 0.20 |
| Dry soil column | | | |
| 0.07 | 0.26 | 0.14 | 0.12 |
| 0.12 | 0.23 | 0.14 | 0.09 |
| 0.19 | 0.20 | 0.14 | 0.06 |
| 0.24 | 0.19 | 0.14 | 0.05 |
| 0.39 | 0.21 | 0.14 | 0.07 |

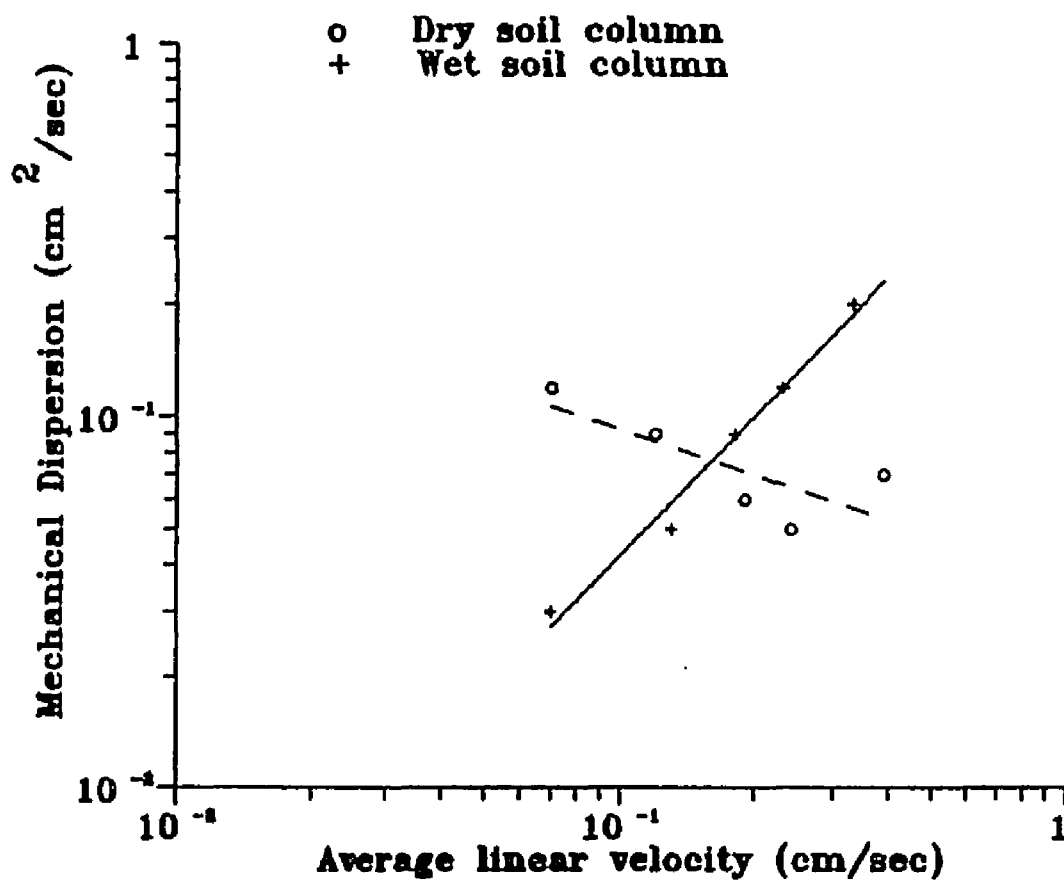


Figure 4.1.3. Mechanical dispersion vs. average linear velocity.

The small values of the coefficient and exponent for the best-fit curve indicate that D_m is independent of velocity in the dry column. This is the result of: (1) relatively large pore openings resulting in less tortuous paths, and (2) porous media diffusion, which is independent of velocity, being the predominant means of dispersive transport at all velocities for helium.

4.2 Saturated Column Experiments

The outflow data obtained from the saturated column experiment (experiment SAT2) were used to generate a breakthrough curve that was analyzed using the single-fluid version of the one-site kinetic model discussed in Chapter 2. Because of leakage problems resulting from diffusion through the teflon feed system, the sorption-limb data were erratic, resulting in a large mass-balance error. Curve-fitting the desorption limb gave a K_p of 0.48 ± 0.16 cm³/g. This is approximately five times greater than the K_p value estimated from the carbon-based partitioning equation (Eqn. 1.2.5) of Schwarzenbach and Westall (1981), 0.10 cm³/g for a soil having an f_{oc} of 0.00097. Because of the large mass-balance error, K_p was not estimated by integrating the area under the breakthrough curve.

4.3 Soil Venting Experiments

Soil venting experiments were run using benzene and *p*-xylene under a variety of conditions that included varying moisture content and flow rate.

The outflow data from the soil-venting experiments were used to generate breakthrough curves. The breakthrough curves were analyzed using: (1) a

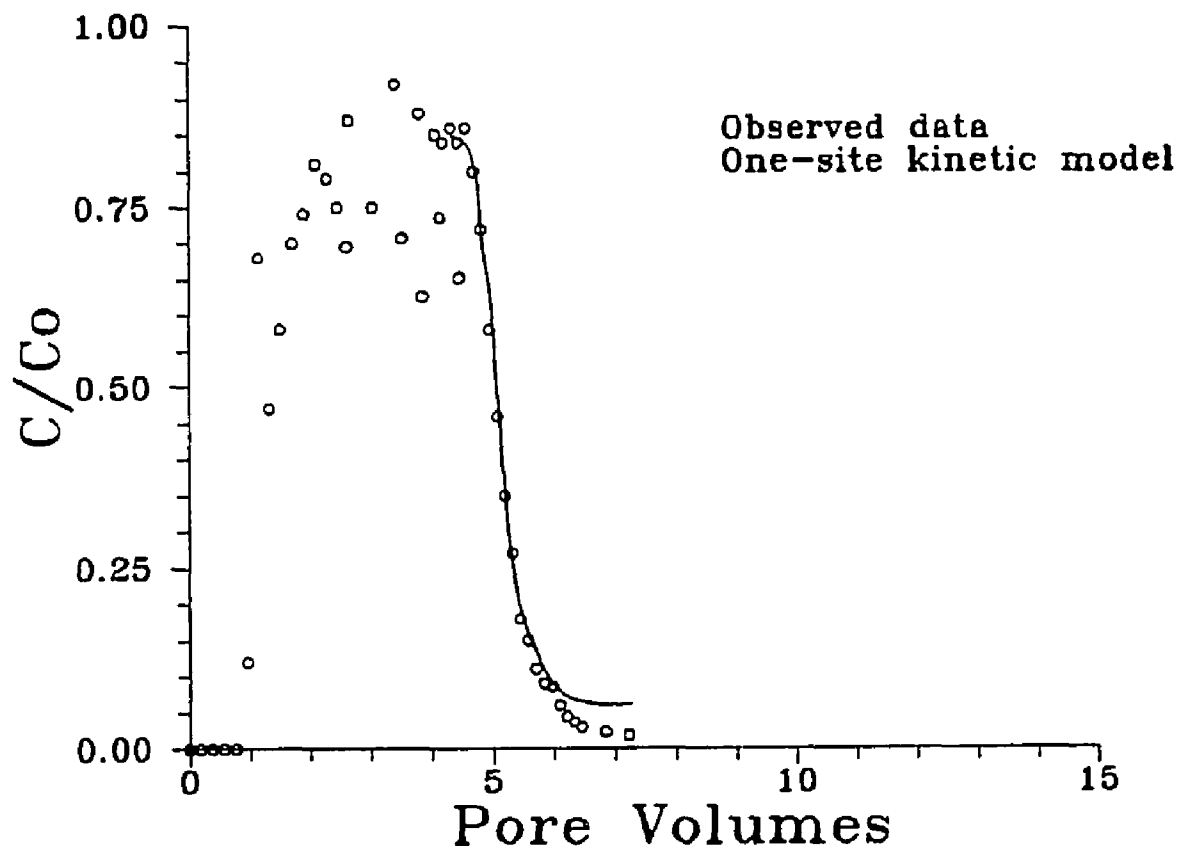


Figure 4.2.1. Observed and fitted breakthrough curves for experiment SAT2 using the one-site kinetic model of van Genuchten (1981). R , T_v , and ω were fitted by the program CFITIM.

planimeter to obtain mass balance errors (the ratio of mass out to mass in), the retardation factor (R), and the partition coefficient (K_p), and (2) the curve-fitting program (CFITIM) to determine kinetic parameters related to slow diffusion through water and slow sorption and desorption from organic matter.

4.3.1. Mass Balances

Figure 4.3.1 illustrates the technique used to determine the mass balance ratios. The total input mass is the area under the input curve ($A + B$), while the total outflow mass is the area under the outflow curve ($B + C$). Planimetric measurements were reproduced twice, and the calculated error was between 5 and 10 percent of the measure area. The mass balance ratios (defined as mass out/mass in) are given in Table 4.3.1.

Mass balance errors for the benzene soil venting experiments were generally reasonable with errors for all experiments no greater than 11 percent except for experiment B15, which had a mass balance error of 19 percent. The mass balance errors for the benzene experiments, with the exception of experiments B8 and B10, result from underestimating the input mass (i.e., mass outflow exceeded mass inflow). This is attributed to condensation of benzene within the apparatus upstream of the soil column or sorption to the teflon fittings during the loading step. Equilibrium mass distribution calculations (calculations based on the equilibrium distribution of mass in each phase using K_H values from Mackay and Shiu (1981) and K_p values obtained from planimetric integration (Table 4.3.1)) show that the concentration in the water was approximately 11 percent

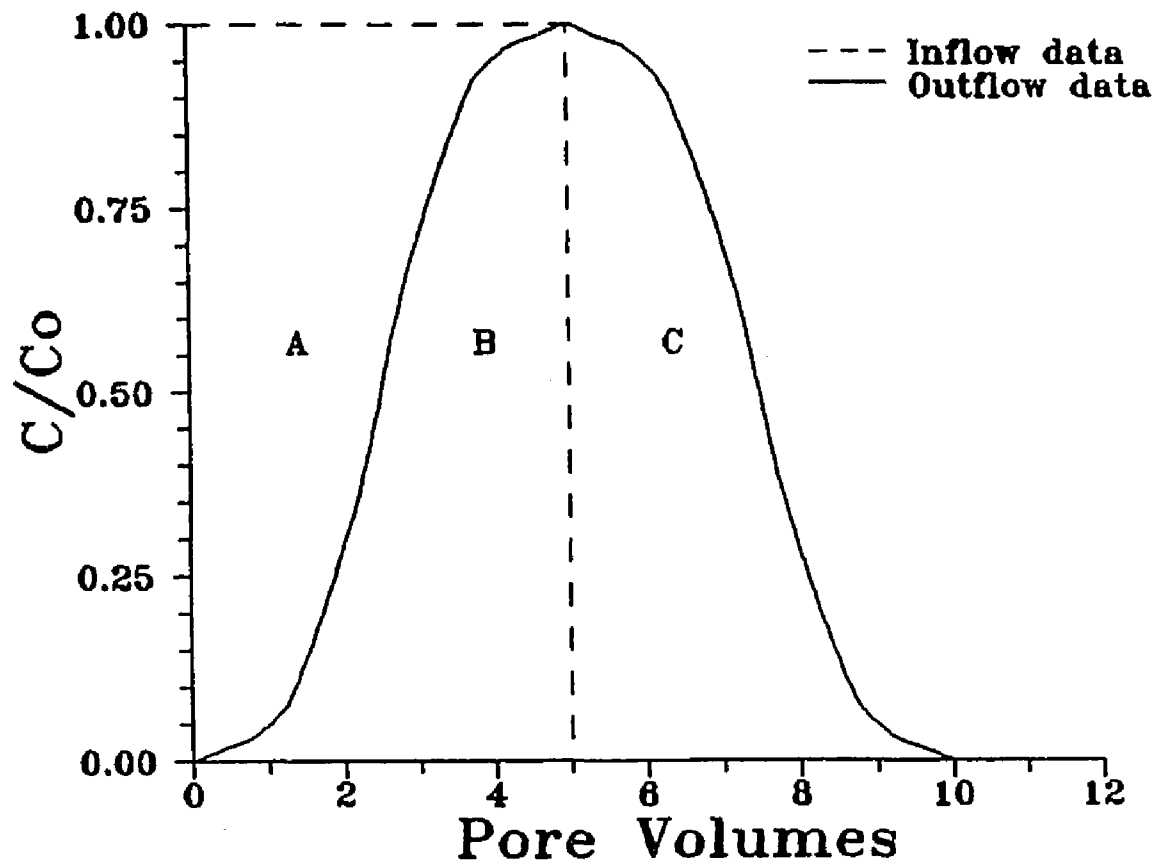


Figure 4.3.1. Hypothetical inflow and outflow curves illustrating the method of calculating mass balance from the area under the curves. $A + B = B + C$ and $A = C = R$, the retardation factor.

Table 4.3.1 Mass Balance Results

| Exp | C _o (mg/l) | mass balance ratio ^a | T ₁ ^b | R ^c | K _p (cm ³ /cm ³) |
|-----------------|--------------------------|---------------------------------------|-----------------------------|----------------|---|
| Wet soil column | | | | | |
| B3 | 348 | 1.03 | 9.4 (9.5) | 1.3 | 0.11 |
| B4 | 374 | 1.09 | 9.4 (9.5) | 1.2 | 0.08 |
| B5 | 426 | 1.04 | 7.1 (7.4) | 1.2 | 0.08 |
| B6 | 389 | 1.04 | 7.4 (7.4) | 1.3 | 0.11 |
| B8 | 149 | 0.96 | 7.4 (8.0) | 1.2 | 0.08 |
| B9 | 152 | 1.11 | 6.7 (7.2) | 1.0 | 0.03 |
| B10 | 105 | 0.99 | 9.4 (9.5) | 1.4 | 0.13 |
| XY5 | 37 | 1.19 | - | - | - |
| XY6 | 33 | 1.26 | - | - | - |
| XY7 | 34 | 1.25 | - | - | - |
| XY8 | 16 | 0.97 | 14 (15) | 5.4 | 1.56 |
| XY9 | 15 | 1.04 | 16 (16) | 4.8 | 1.35 |
| XY10 | 13 | 0.92 | 12 (12) | 5.5 | 1.59 |
| Dry soil column | | | | | |
| B15 | 357 | 1.19 | - | - | - |
| B16 | 368 | 1.04 | 27 (25) | 3.6 | 0.66 |
| B17 | 344 | 1.11 | 21 (18) | 2.4 | 0.37 |
| XY1 | 35 | 1.16 | - | - | - |
| XY2 | 45 | 1.18 | - | - | - |
| XY3 | 35 | 1.20 | - | - | - |
| XY4 | 32 | 1.28 | - | - | - |

^a Defined as mass out/mass in.

^b Measured (planimetric) values given in parentheses.
Fitted values of T₁ are the same for all models.

^c Average R = (A + C)/2 (see Figure 4.3.1).

below solubility for all high concentration benzene experiments (with the exception of B5), implying that there was no liquid benzene present in the soil column. (The low concentration benzene experiments had aqueous phase concentrations that were approximately 66 percent below solubility.) The mass balance errors for B8 and B10 are small (4 percent and 1 percent, respectively).

Mass balance errors for the *p*-xylene soil venting experiments were variable with errors ranging from 3 percent to 28 percent, with the average error being 17 percent. The mass balance errors associated with the *p*-xylene soil venting experiments are similar to those of the benzene soil venting experiments in that the mass output exceeded the mass input for all experiments with the exception of XY8 and XY10. *p*-xylene, which has a lower vapor pressure, as well as a higher K_{ow} than benzene, is more likely to condense. Equilibrium mass distribution calculations show that the concentration of *p*-xylene in the water was approximately 35 and 74 percent below solubility for the high and low concentration experiments, respectively, thus implying that there was no liquid *p*-xylene present in the soil column. The mass balance errors for the low concentration experiments (XY8, XY9, and XY10) are much lower than for the high concentration experiments.

Mass balance is important in that breakthrough curves demonstrating poor mass balance are difficult to reproduce using analytical solutions. Therefore, T_r was allowed to vary in order to achieve mass balance. The observed and fitted pulse values (T_r) differ proportionally to the size of the mass balance ratio. The value of R , and hence, K_p , may also vary in response to mass balance errors.

Adjusted and observed T_1 values are shown in Table 4.3.1. Since mass balance is independent of the model used, the fitted values of T_1 are the same (within 1 to 6 percent) for all models.

The area between the inflow and outflow curves (area 'A' of Figure 4.3.1) is R, the retardation factor. This is true for both the sorption and desorption limbs ($A = C$ for mass balance). Because of mass balance errors, the average R ($(A + C)/2$) is reported as the observed value in Table 4.3.1. Outflow concentrations did not reach inflow concentration levels during experiments XY1, XY2, XY6, and XY8. This indicates that the retardation factor (R) determined from these experiments are underestimates.

Using the average value of R obtained by planimetric integration, C_o , and the air-filled pore volume, the immobilized (dissolved and sorbed) mass can be determined. The mass in the air can be determined using C_o , θ_a , and the air-filled pore volume. The dissolved concentration (C_w) is estimated using K_H and C_o . The dissolved mass is estimated using C_w , θ_w , and the air-filled pore volume. The mass in the soil is the immobilized mass minus the dissolved mass. The concentration in the soil is estimated using the bulk density and the density of the quartz sand (2.65 g/cm^3) to determine the volume of soil in the column. K_p can be then determined. K_p values estimated from the planimetric R values are listed in Table 4.3.1.

Since the concentrations in, and the volumes of, each phase can be determined, the relative distribution of mass among the phases for both compounds at both moisture contents at equilibrium can be estimated. Because the

values of K_p estimated using planimetric integration varied (K_p benzene = 0.20 ± 0.18 cm³/cm³, K_p *p*-xylene = 1.50 ± 0.13 cm³/cm³; the error representing one standard deviation), the carbon-based K_p values of Schwarzenbach and Westall (1981) were used to determine the equilibrium mass distribution in each phase (Table 4.3.2).

4.3.2 Curve-fitting Results

Large mass balance errors significantly bias the parameter values obtained from the curve-fitting program for the models used. Experiments having mass balance ratios between 0.85 and 1.15 will be the only ones analyzed and discussed. (The dry column *p*-xylene experiments will not be discussed).

Breakthrough curves obtained from the wet column experiments exhibited more tailing, indicating that slow diffusion is important.

Tailing for the dry column and wet columns was also seen to increase with velocity.

All experiments were fitted using the one-site kinetic model using a three-parameter curve-fitting scheme in which P was fixed, while R , T_1 , and ω were allowed to vary.

4.3.2.1 Equilibrium model. Two modeling schemes were used when attempting to fit the data with the equilibrium model subroutine of CFITIM. The first was a three-parameter curve-fitting scheme in which all three parameters of the equilibrium model (P , R , and T_1) were determined by the program. The second scheme, a two-parameter curve-fitting scheme, involved fixing the

Table 4.3.2 Equilibrium Mass Distribution of Benzene and *p*-Xylene in the Soil, Aqueous, and Vapor Phases^{a,b}

| Compound | Column | Air (%) | Water (%) | Soil (%) |
|------------------|--------|---------|-----------|----------|
| Benzene | wet | 10.6 | 46.0 | 43.4 |
| Benzene | dry | 20.0 | 28.0 | 52.0 |
| <i>p</i> -xylene | wet | 4.5 | 15.0 | 80.5 |
| <i>p</i> -xylene | dry | 7.4 | 8.3 | 84.3 |

^a . Reported as the percentage of total mass in the system.

^b Values obtained using the theoretical (carbon-based partitioning equation) K_p (0.10 cm³/g for benzene and 0.56 cm³/g for *p*-xylene). Calculation assumes $f_{oc} = 0.00097$.

value of P based on results from the helium dispersion studies and allowing the program to vary only R and T_1 .

In the first scheme, a lower than expected P value indicates that transport under a given set of conditions (moisture content, velocity, and concentration) is hindered by a non-equilibrium process. A decrease in P serves to broaden the breakthrough curve by increasing dispersion (Figure 2.2.2). Therefore, the equilibrium model can fit tailing on breakthrough curves due to non-equilibrium processes by increasing dispersion. The values of D were increased for all cases which suggests that non-equilibrium processes are important (Table 4.3.3).

Plots of D/D_0 versus $v_p d/D_0$ for benzene and *p*-xylene experiments were prepared using the results of the equilibrium model in order to analyze tailing in the breakthrough curves (Figure 4.3.2). The parameter d is the effective grain diameter which was estimated using the average aggregate grain diameter as determined by dry sieving (0.0505 cm) and the moisture content. The value of d was 0.0548 cm for the wet column and 0.0528 cm for the dry column.

Figure 4.3.2 shows that both compounds exhibit tailing (the value of D/D_0 for the compounds is greater than that for helium) at both moisture contents, and that tailing in the wet column is greater than in the dry column. The figure also shows that benzene and *p*-xylene exhibit similar tailing at both moisture contents.

The second scheme (fixing P and allowing R and T_1 to vary) was used in order to determine if the equilibrium model adequately describes any of the

Table 4.3.3 Curve-fitting Results for the Benzene and *p*-Xylene Soil Venting Experiments using the Equilibrium Model^a

| Exp | SSQ | v_a (cm/sec) | R | T_1 | $D \times 10^{-2}$ (cm ² /sec ^b) |
|------------------------|------|-------------------|-----------|-------------|--|
| Wet soil column | | | | | |
| B3 | 0.06 | 0.19 | 1.1 (1.3) | 9.4 (9.5) | 237.5 (10.7) |
| B4 | 0.12 | 0.19 | 0.9 (1.2) | 9.4 (9.5) | 167.6 (10.7) |
| B5 | 0.12 | 0.30 | 0.7 (1.2) | 7.1 (7.4) | 473.7 (18.9) |
| B6 | 0.09 | 0.10 | 0.9 (1.3) | 7.4 (7.4) | 68.2 (5.1) |
| B8 | 0.12 | 0.10 | 1.2 (1.2) | 7.4 (8.0) | 62.5 (5.1) |
| B9 | 0.14 | 0.29 | 0.7 (1.0) | 6.7 (7.2) | 334.6 (18.1) |
| B10 | 0.30 | 0.19 | 1.1 (1.4) | 9.4 (9.5) | 247.8 (10.7) |
| Dry soil column | | | | | |
| B16 | 0.74 | 0.23 | 2.5 (3.6) | 27.0 (25.0) | 43.7 (9.6) |
| B17 | 0.55 | 0.33 | 1.5 (2.4) | 21.0 (18.0) | 145.6 (9.6) |
| Wet soil column | | | | | |
| XY8 | 0.38 | 0.19 | 6.9 (5.4) | 14 (15) | 158.3 (10.5) |
| XY9 | 0.07 | 0.30 | 4.0 (4.8) | 16 (16) | 250.0 (18.7) |
| XY10 | 0.13 | 0.11 | 5.1 (5.5) | 12 (12) | 49.3 (5.5) |

^a P, R, and T_1 were fitted by the program.

^b Calculated values are given in parentheses.

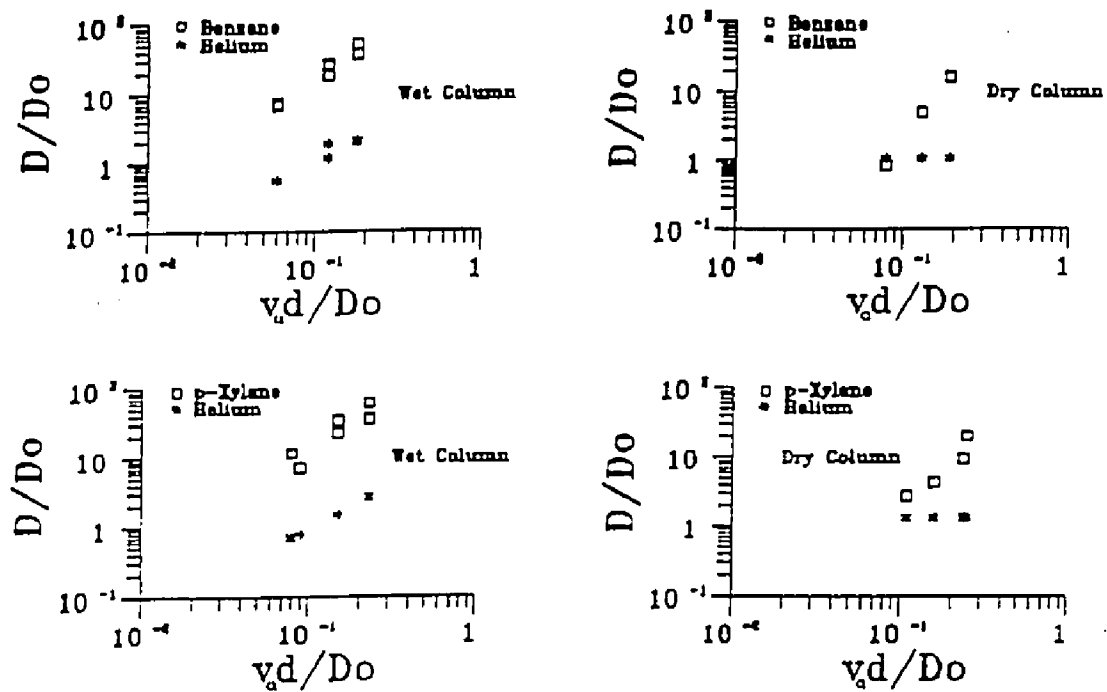


Figure 4.3.2. D/D_0 vs. v_0d/D_0 for the benzene and *p*-xylene using the equilibrium model. P, R, and T, were fitted by the program CFITIM.

breakthrough curves. Fits obtained using this scheme were poor for both the benzene and *p*-xylene venting experiments.

4.3.2.2 One-site kinetic model. A curve-fitting scheme in which P was fixed and R , T , and ω were fitted was used to obtain transport and kinetic parameters. The curve-fitting results for the experiments with good mass balance ratios are listed in Table 4.3.4.

Values for R obtained from the one-site kinetic model were in agreement with those calculated by means of planimetric integration.

ω values are observed to be lowest for the high velocity experiments and highest for the low velocity experiments. This suggests that tailing increases as velocity increases.

Figures 4.3.3 and 4.3.4 are representative plots of observed and fitted data for the wet and dry column benzene experiments, respectively. The remaining plots are contained in Appendix B. Figure 4.3.5 is a representative plot of observed and fitted data for the wet column *p*-xylene experiments. The remaining plots (XY8 and XY10) can be found in Appendix C.

Although the SSQs were relatively large, tailing was reproduced well because most of the error was due to poor fits to data on the steepest portion of the breakthrough curve.

The dimensional parameters obtained using the dimensionless parameters fitted by the one-site kinetic model are listed in Table 4.3.5.

Fitted K_p values were within a factor of two of the calculated (planimetric integration) values. The fitted values were also within a factor of two of the

Table 4.3.4 Dimensionless Parameters Obtained Using the One-site Kinetic Model^a

| Exp | SSQ | v_a (cm/sec) | R | T_1 | ω |
|------------------------------|------|-------------------|---------------------|-------------|----------|
| Wet soil column ^b | | | | | |
| B3 | 0.25 | 0.19 | 1.5 \pm 0.1 (1.3) | 9.4 (9.5) | 0.3 |
| B4 | 1.35 | 0.19 | 1.4 \pm 0.4 (1.2) | 9.4 (9.5) | 0.2 |
| B5 | 2.36 | 0.30 | 1.4 \pm 0.4 (1.2) | 7.1 (7.4) | 0.2 |
| B6 | 1.00 | 0.10 | 1.4 \pm 0.2 (1.3) | 7.4 (7.4) | 0.3 |
| B8 | 0.50 | 0.10 | 1.5 \pm 0.1 (1.2) | 7.4 (8.0) | 0.5 |
| B9 | 2.77 | 0.29 | 1.4 \pm 0.4 (1.0) | 6.7 (7.2) | 0.2 |
| B10 | 1.41 | 0.19 | 1.8 \pm 0.5 (1.4) | 9.4 (9.5) | 0.3 |
| XY8 | 0.49 | 0.19 | 6.2 \pm 0.2 (5.4) | 14.0 (15.0) | 4.0 |
| XY9 | 0.18 | 0.30 | 3.8 \pm 0.1 (4.8) | 16.0 (16.0) | 3.2 |
| XY10 | 0.33 | 0.11 | 5.0 \pm 0.1 (5.5) | 12.0 (12.0) | 5.4 |
| Dry soil column ^c | | | | | |
| B16 | 0.76 | 0.23 | 2.5 \pm 0.2 (3.6) | 27.0 (25.0) | 8.0 |
| B17 | 0.49 | 0.33 | 1.6 \pm 0.2 (2.4) | 21.0 (18.0) | 0.6 |

^a Calculated values (Table 4.3.1) in parenthesis.

^b P was fixed using Eqn. 4.1.3 and D_a for the compound.

^c P was fixed using average dry column $D_m = 0.08 \text{ cm}^2/\text{sec}$ (see Table 4.1.3).

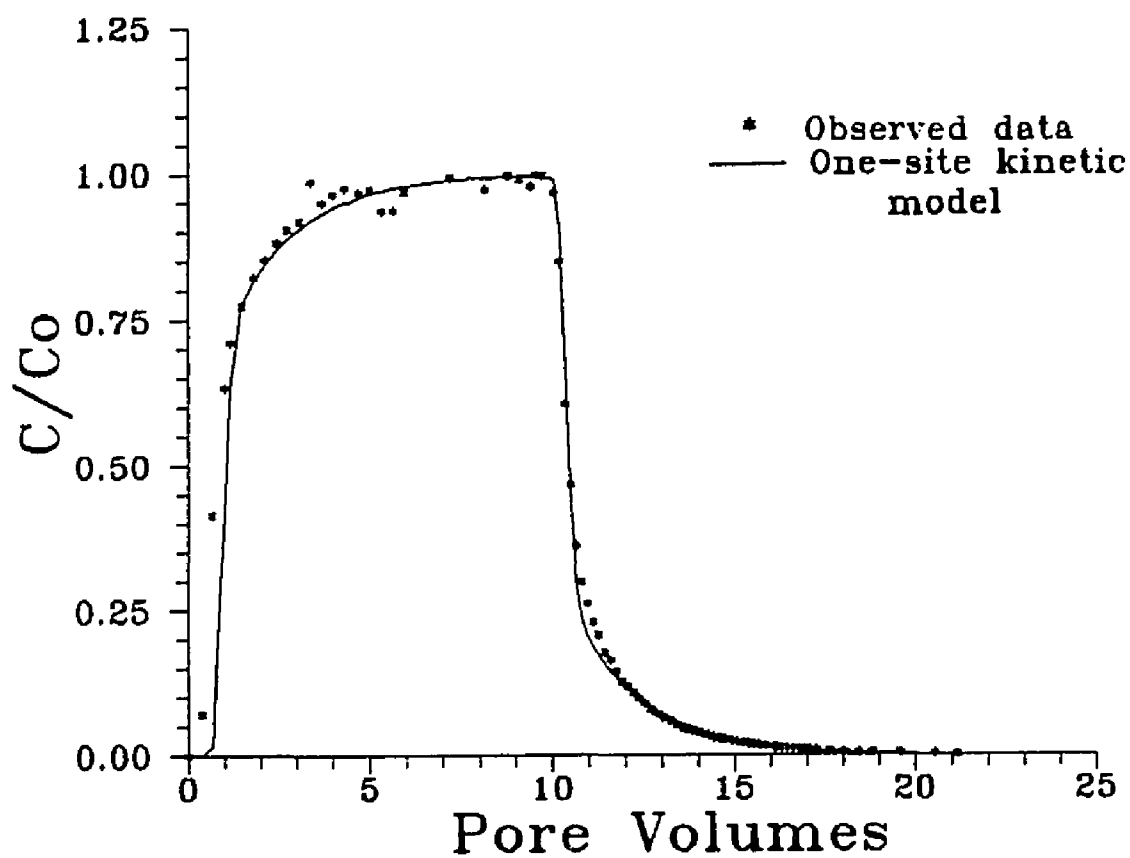


Figure 4.3.3. Observed and fitted breakthrough curves for wet column experiment B3 using the one-site kinetic model. R , T , and ω were fitted by the program CFITIM. P was fixed at 53.1.

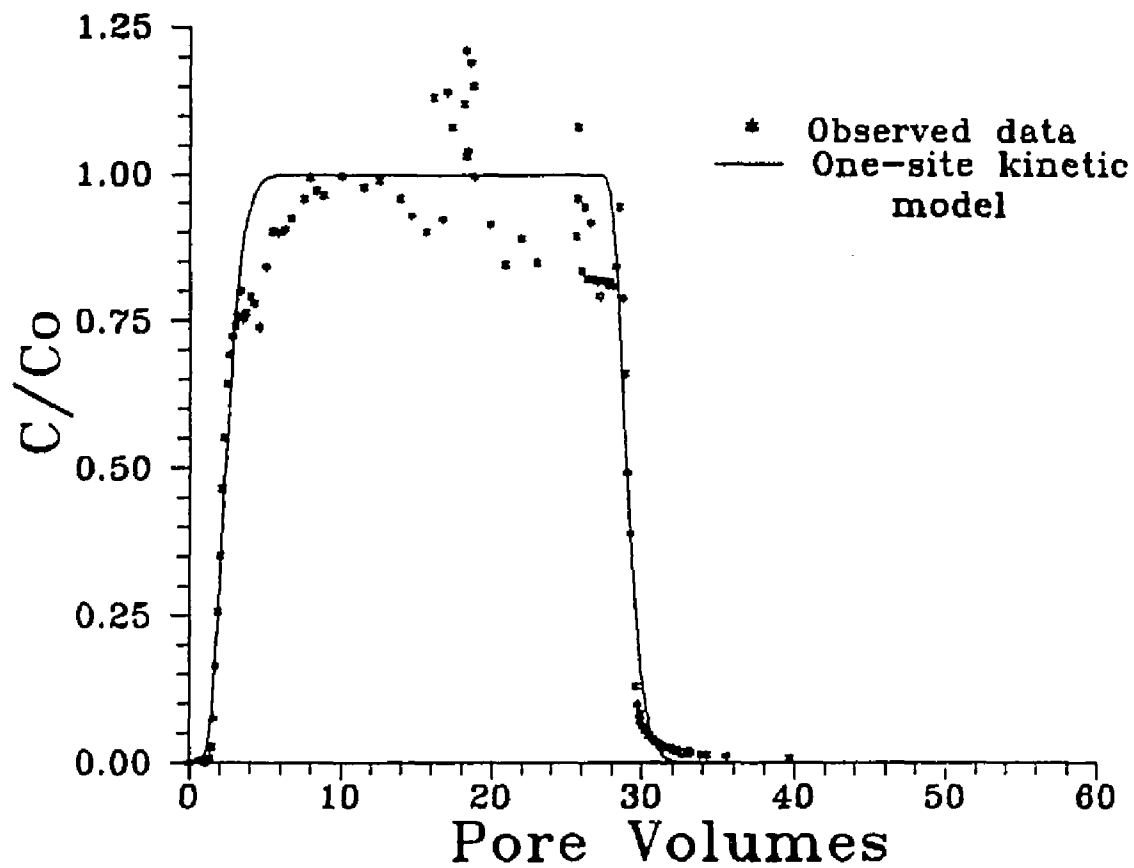


Figure 4.3.4. Observed and fitted breakthrough curves for dry column experiment B17 using the one-site kinetic model. R , T , and ω were fitted by the program CFITIM. P was fixed at 102.6.

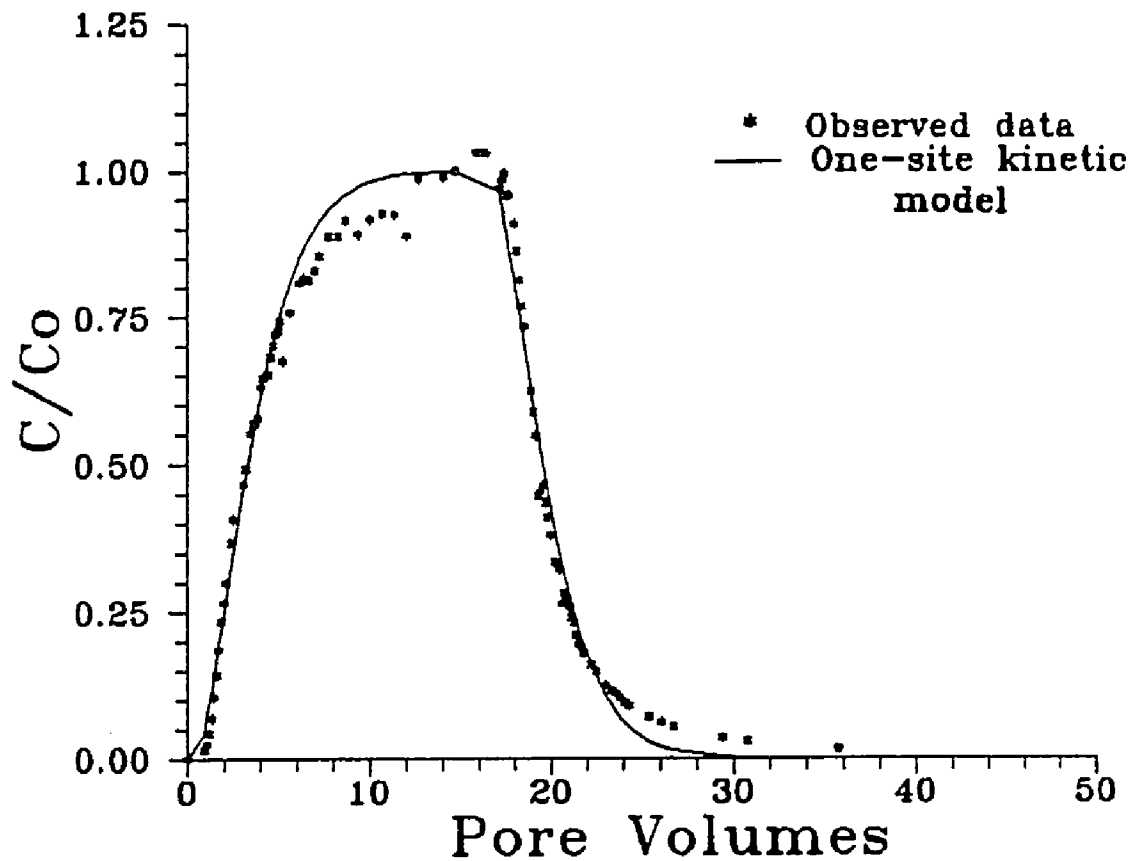


Figure 4.3.5. Observed and fitted breakthrough curves for wet column experiment XY9 using the one-site kinetic model. R , T_1 , and ω were fitted by the program by CFITIM. P was fixed at 48.2.

Table 4.3.5 Dimensional Partitioning and Kinetic Parameters Obtained using the One-site Kinetic Model^a.

| Exp | SSQ | K_p^b (cm ³ /cm ³) | $k_t \times 10^{-3}$ (sec ⁻¹) | $k_b \times 10^{-4}$ (sec ⁻¹) |
|-----------------|------|--|--|--|
| Wet soil column | | | | |
| B3 | 0.25 | 0.07 ± 0.01 (0.04) | 1.9 | 7.8 |
| B4 | 1.35 | 0.05 ± 0.06 (0.03) | 1.3 | 6.5 |
| B5 | 2.36 | 0.05 ± 0.06 (0.03) | 2.0 | 10.3 |
| B6 | 1.00 | 0.05 ± 0.03 (0.04) | 1.0 | 5.2 |
| B8 | 0.50 | 0.07 ± 0.01 (0.03) | 1.7 | 6.9 |
| B9 | 2.77 | 0.05 ± 0.06 (0.01) | 1.9 | 10.0 |
| B10 | 1.41 | 0.11 ± 0.07 (0.05) | 1.9 | 4.9 |
| XY8 | 0.49 | 0.69 ± 0.03 (0.59) | 25.1 | 10.5 |
| XY9 | 0.18 | 0.37 ± 0.02 (0.51) | 32.1 | 24.6 |
| XY10 | 0.33 | 0.53 ± 0.02 (0.60) | 20.0 | 10.6 |
| Dry soil column | | | | |
| B16 | 0.76 | 0.15 ± 0.02 (0.25) | 61.0 | 183.0 |
| B17 | 0.49 | 0.06 ± 0.02 (0.14) | 6.6 | 49.2 |

^a P fixed and R, T₁, and ω fitted.

^b Calculated values (Table 4.3.1) in parentheses.

values calculated using the carbon-based partitioning equation of Schwarzenbach and Westall (1981): $0.10 \text{ cm}^3/\text{g}$ for benzene and 0.56 for *p*-xylene for a soil with an f_{oc} of 0.00097 .

The average half-lives for sorption and desorption of benzene in the wet column were 7 and 17 minutes, respectively. Corresponding half-lives in the dry column were 1 and 1.5 minutes, respectively. The difference in the values indicates that another process (perhaps slow aqueous diffusion) is important as reaction rate coefficients should be independent of moisture content.

The average half-lives for sorption and desorption of *p*-xylene in the wet column were 0.5 and 9 minutes, respectively. The desorption half-life for *p*-xylene is an underestimate since tailing was underestimated. Because of its greater K_p , *p*-xylene is expected to desorb more slowly than benzene.

4.3.2.3 Slow diffusion model. The slow diffusion model (which, like the one-site kinetic model, has four parameters) was also used to fit the dry column benzene experiments. A curve-fitting scheme in which P was fixed and R , T_1 , and ω were fitted was used to obtain transport and kinetic parameters. Figure 4.3.6 is a representative plot of the observed and fitted data for the dry column experiments. Curve-fitting results are given in Table 4.3.6.

The slow diffusion model underestimated tailing in the wet column for both compounds, suggesting that other process(es) were operative at the higher moisture content (perhaps slow reactions at the binding sites). Since the analytical solution to the slow diffusion and one-site kinetic models are identical, the

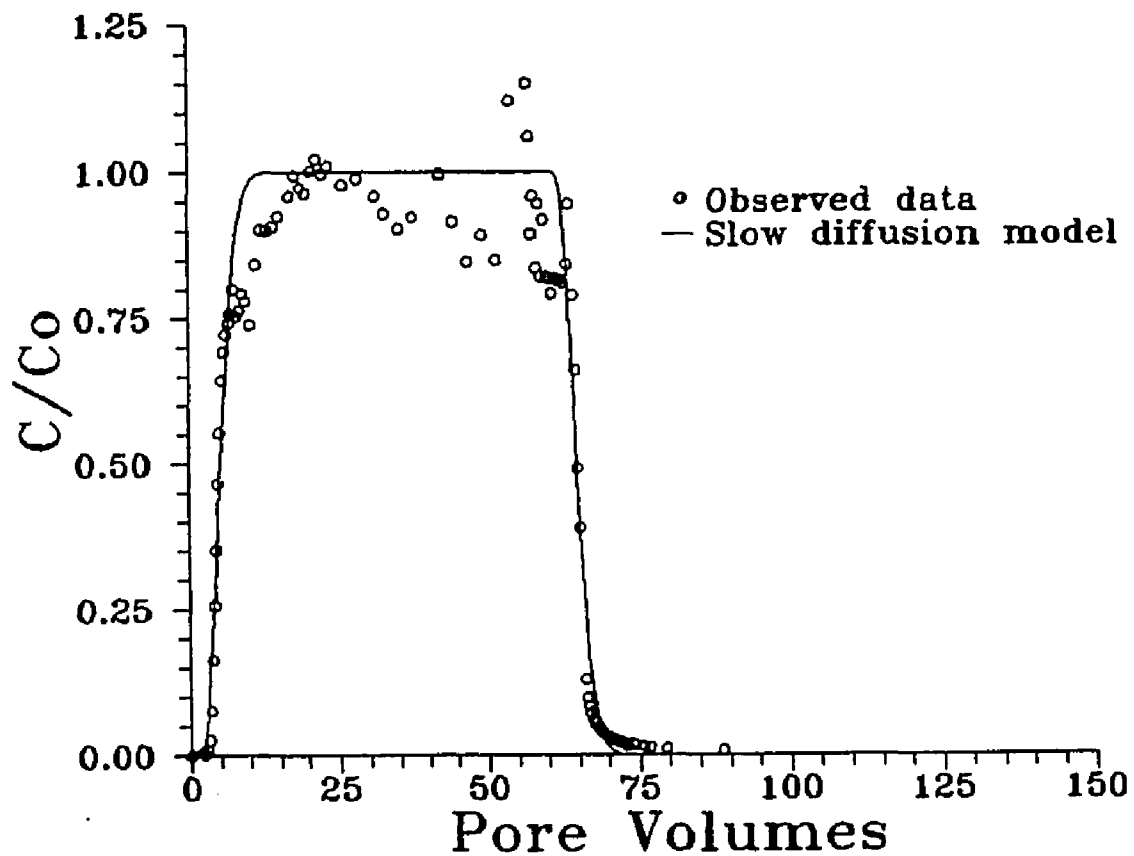


Figure 4.3.6. Observed and fitted breakthrough curves for dry column experiment B17 using the slow diffusion model. R , T , and ω were fitted by the program by CFITIM. P was fixed at 102.6.

Table 4.3.6 Dimensionless Parameters for the Dry Column Benzene Soil Venting Experiments using the Slow Diffusion Model^{a,b}.

| Exp | SSQ | R | T ₁ | ω |
|-----|------|-----------------|----------------|------|
| B16 | 0.76 | 5.5 ± 0.3 (8.0) | 59 (56) | 15.0 |
| B17 | 0.59 | 3.3 ± 0.3 (5.3) | 45 (41) | 4.4 |

^a P was fixed and R, T₁, and ω were fitted by the program.

^b Calculated values (Table 4.3.1) given in parenthesis.

poor fit indicates that the curve-fitting scheme is sensitive to shifting the break-through curves by means of different T_1 expressions.

R values were within a factor of two of those calculated by planimetric integration.

Dimensional parameters obtained using the dimensionless ones obtained using the slow diffusion model are presented in Table 4.3.7.

Fitted K_p values were within a factor of four of both the calculated and carbon-based partitioning values.

The average half-life for diffusion (calculated using α_w) is 0.5 minutes. This is approximately the same as the sorption and desorption half-lives obtained using the one-site kinetic model.

Calculations based on the aqueous phase diffusion coefficient of benzene (9.7×10^{-6} cm²/sec; Welty et al., 1976) and the average α_w show the diffusive path length to be 0.02 cm. Since this is an order of magnitude greater than the water film thickness (i.e., the effective aggregate diameter (0.0528 cm) minus the aggregate diameter (0.0505 cm) = 0.0023 cm), it is concluded that intra-aggregate diffusion must be considered if the slow diffusion model is to be used to describe these experiments. If diffusion is limited to the external film of water surrounding the aggregate, it is not a rate-limiting step since it is estimated that the diffusive path length must be at least 0.006 cm in order for aqueous diffusion of benzene to be rate-limiting.

In an effort to fit the tailing in the wet column, a minimum ω was calculated assuming a diffusive path length that was one-half the effective diameter

Table 4.3.7 Dimensional Partitioning and Kinetic Parameters for the Dry Column Benzene Soil Venting Experiments using the Slow Diffusion Model^a.

| Exp | SSQ | K_p (cm ³ /cm ³) ^b | $\alpha_w \times 10^{-3}$ (sec ⁻¹) |
|-----------------|------|---|---|
| Dry soil column | | | |
| B16 | 0.76 | 0.10 ± 0.02 (0.36) | 25.6 |
| B17 | 0.59 | 0.03 ± 0.02 (0.11) | 21.0 |

^a P fixed and R, T_v, and ω fitted.

^b Calculated values (Table 4.3.1) in parenthesis.

(d). This resulted in a poor fit. Poor fits also resulted when ω was fixed at values one and two orders of magnitude less than the minimum value.

4.3.2.4 Two-compartment model. Analytical evidence (i.e., the one-site kinetic model gives moisture content dependent half-lives and Figure 4.3.2) showed tailing in the wet column to be greater than in the dry column. It is expected that multiple processes are occurring in the wet column (e.g., slow reactions at the binding sites due to the hydrophobicity of VOCs, slow diffusion, as well as slow sorption and desorption). These processes must be considered when describing the wet column experiments. For this reason, the two-compartment model (which assumes equilibrium is approached slowly at some sites) was used to fit the wet column breakthrough curves.

A four-parameter curve-fitting scheme was used when fitting the data with the two-compartment model. P was fixed and R , T , ω , and β were fitted by the program.

The two-compartment model was successful in reproducing the wet column benzene breakthrough curves. However, F values obtained using the two-compartment model were out of the specified range (0 to 1); therefore, analysis of the wet column benzene breakthrough curves is restricted to the one-site kinetic model. Tailing in the dry column experiments was overestimated by the two-compartment model.

The two-compartment model was successful in reproducing the wet column *p*-xylene breakthrough curves. The curve-fitting results are listed in Table 4.3.8.

Table 4.3.8 Dimensionless Parameters for the *p*-Xylene Soil Venting Experiments using the Two-compartment Model^{a,b}

| Exp | SSQ | R ^c | T ₁ | β | ω |
|------|------|----------------|----------------|---------|----------|
| XY8 | 0.48 | 30.3 (25.0) | 63 (71) | 0.30 | 3.0 |
| XY9 | 0.06 | 18.7 (22.5) | 76 (75) | 0.50 | 1.1 |
| XY10 | 0.07 | 24.7 (25.5) | 56 (57) | 0.57 | 1.1 |

^a P was fixed and R, T₁, β , and ω were fitted by the program.

^b Calculated values (see Table 4.3.1) given in parentheses.

Figure 4.3.7 shows a representative plot of the observed and fitted data for the wet column *p*-xylene experiments using the two-compartment model. The remaining *p*-xylene plots (XY8 and XY10) are contained in Appendix C. The large SSQ for XY8 is the result of erratic data at the top of the breakthrough curve and does not reflect a failure in the prediction of observed tailing. Dimensional parameters calculated using the dimensionless parameters are given in Table 4.3.9.

Fitted K_p values were within a factor of two of both the calculated and carbon-based partitioning values.

The average value of k_1 for the low concentration experiments was 0.016 sec^{-1} , which gives a half-life of 0.7 minutes. The average value of k_2 for the low concentration experiments was 0.0008 sec^{-1} , which gives a half-life of 15 minutes. These values are approximately the same as those obtained using the one-site kinetic model; therefore, the only additional information obtained by using the two-compartment is an estimate of F .

The largest F value for the low concentration *p*-xylene venting experiments is obtained for the lowest velocity experiment (XY10), while smaller F values are obtained for the higher velocity experiments (XY8 and XY9). This is expected since equilibrium conditions, which are suggested by larger F values, are approached as velocity decreases.

Table 4.3.9 Dimensional Partitioning and Kinetic Parameters for the *p*-Xylene Soil Venting Experiments using the Two-compartment Model^a

| Exp | SSQ | K_p^b (cm ³ /cm ³) | $k_1 \times 10^{-3}$ (sec ⁻¹) | $k_b \times 10^{-3}$ (sec ⁻¹) | F |
|------|------|--|--|--|-----|
| XY8 | 0.48 | 0.73 ± 0.05 (0.55) | 23.8 | 0.9 | 0.2 |
| XY9 | 0.06 | 0.40 ± 0.02 (0.53) | 15.7 | 1.2 | 0.3 |
| XY10 | 0.07 | 0.57 ± 0.02 (0.68) | 8.0 | 0.4 | 0.5 |

^a P was fixed and R, T, β , and ω were fitted by the program.

^b Calculated values (Table 4.3.1) in parentheses.

CHAPTER 5

DISCUSSION

5.1 Helium Tracer Experiments

Results show the D_m for the wet soil column increases with increasing velocity. D_m for the dry column is independent of velocity because porous media diffusion (D_0), which is independent of velocity, is the primary means of dispersive transport at all velocities for helium (Table 4.1.3).

Freeze and Cherry (1979) maintain that exponents of v_d between 1 and 2 imply velocity dependent mechanical dispersion for aqueous phase transport. This axiom can be extended to vapor phase transport provided that flow is incompressible. Flow versus pressure experiments showed the flow to be incompressible; therefore, the power functions (Eqns. 4.1.3 and 4.1.4) indicate that the wet column has velocity dependent mechanical dispersion while the dry column has a mechanical dispersion independent of velocity. The negative exponent obtained for the dry column is the result of the erratic behavior of the data and the resulting best-fit line and is therefore not interpreted as a trend.

The values obtained for v_d/D_0 and D/D_0 (Figure 4.3.2) indicate that the dispersive behavior of both columns lie in the "transition zone" (Zone II) described by Bear (1979). This zone marks the transition from velocity independent mechanical dispersion to velocity dependent mechanical dispersion.

Due to heterogeneities on the field scale, mechanical dispersion coefficients are often orders of magnitude greater than those obtained on the laboratory scale using homogeneous porous media. Therefore, it is unlikely that these results are

applicable on the field scale. For field scale experiments, dispersion should be calculated for the system being studied.

5.2 Saturated Column Experiment

The one-site kinetic model overestimated tailing in the desorption limb of experiment SAT2 (Figure 4.2.1). Furthermore, the benzene K_p obtained from the saturated column experiment (0.48 ± 0.16 cm³/g) using this model is higher than that predicted by the carbon-based partitioning equation of Schwarzenbach and Westall (1981) (0.10 cm³/g) for a soil having a f_{oc} of 0.00097. It is believed that the erroneous K_p value results from the mass balance error and erratic data near the top of the desorption limb.

The mass balance error could have been the result of a faulty feed system. The feed system was a teflon bag containing the contaminant in solution. Diffusion of the VOC through the bag resulted in a gradual decrease in the input concentration throughout the experiment. A glass reservoir fitted with stainless steel or glass stoppers could eliminate this problem.

5.3 Soil Venting Experiments

5.3.1 Mass Balances

Due to large mass balance errors (16 to 28 percent), none of the dry column *p*-xylene breakthrough curves were analyzed.

The R values for the dry column exceed those of the wet column for both compounds. However, this is difficult to state conclusively due to mass balance

errors. Since retardation is observed to increase with an increase in the mass fraction present in the soil (i.e., a decrease in moisture content), this suggests that the soil phase contributes to retardation more than the aqueous phase.

The larger R values indicates that *p*-xylene partitions to the immobile phases (water and soil) to a greater extent than benzene. This result is demonstrated by equilibrium mass distribution calculations (Table 4.3.2) which show that 80 and 89 percent of the benzene is present in the immobile (aqueous and soil) phase for the dry and wet column and 89 percent is immobilized in the wet columns, respectively. Ninety-three and 96 percent of the *p*-xylene is located in the immobile phases in the dry and wet columns, respectively.

The benzene K_p values obtained by planimetric integration of breakthrough curves displaying small mass balance errors were within a factor of two of the theoretical benzene K_p calculated using the carbon-based partitioning equation of Schwarzenbach and Westall (1981) which is $0.10 \text{ cm}^3/\text{g}$ for a soil having a f_{oc} of 0.00097.

The K_p values obtained by planimetric integration for the low concentration, low mass balance error, *p*-xylene experiments agree with the calculated (carbon-based partitioning equation) *p*-xylene K_p which is determined to be $0.56 \text{ cm}^3/\text{g}$.

Table 4.3.2 shows that at higher moisture contents, a greater percentage of mass is present in the aqueous phase; therefore, moisture dependent rate-limiting processes (such as slow intra- or inter-aggregate diffusion through the aqueous phase) may be important in these conditions. This is intuitively appealing since,

at higher moisture contents, diffusive path lengths and hence, time scales of diffusion, will increase.

5.3.2 Curve-fitting Results

Equilibrium modeling results indicated that tailing in the wet column was greater than in the dry column (Figure 4.3.2). The equilibrium model using the known dispersion values underestimated tailing in all experiments. Therefore, the breakthrough curves were modeled using kinetic (non-equilibrium) models.

The one-site kinetic model using the three-parameter curve-fitting scheme gave good fits to data for all breakthrough curves. Time scales for sorption and desorption were on the order of minutes. The corresponding ω values for these time scales are one to two orders of magnitude less than the equilibrium ω value of 50 (Schwarzenbach and Westall, 1981), suggesting that these systems are indeed non-equilibrium systems.

The moisture content dependence of the kinetic time scales indicates that slow sorption and desorption are not the only slow processes occurring. Slow aqueous phase diffusion may account for the difference in time scales since the time scale of slow diffusion increases with moisture content as a result of the increase in diffusive path length. The sorption and desorption time scales for the wet column were approximately 6 and 15.5 minutes greater than those for the dry column. This suggests that the one-site kinetic model does not provide accurate parameter estimates at the higher moisture content since sorption and desorption rate coefficients should be independent of moisture content.

The slow diffusion model can be used to fit the dry column (benzene) experiments. A reasonable interpretation of this result is that intra-aggregate aqueous phase diffusion is occurring. The estimated time scale for aqueous phase diffusion in the dry column (0.5 minutes) corresponds to a diffusive path length (0.02 cm) that is an order of magnitude longer than the water film thickness (0.0023 cm). The diffusive time scale obtained using the slow diffusion model is approximately equal to the kinetic time scales given by the one-site kinetic model.

Wu and Gschwend (1988) formulated a model that accounted for tailing using intra-aggregate diffusion. Their model contains an effective diffusion coefficient that is related to K_p . Their model worked well for sandy soils with a narrow aggregate size distribution, such as the one used for this study.

The slow diffusion model underestimated observed tailing in the wet column breakthrough curves implying that are other slow processes occurring.

The two-compartment model provided good fits to the wet column *p*-xylene breakthrough curves as well as *F* values that were in the specified range. However, kinetic parameters were approximately the same as those given by the one-site kinetic model; therefore, no additional kinetic information related to aqueous diffusion and reactions (except for *F* values) was obtained by using the two-compartment model.

To determine if the time scales of the rate-limiting process determined in the column experiment would be important on to field-scale operations, a calculation can be made using reasonable values for air flow and radius of influence for an extraction well (30 ft³/sec and 3 feet, respectively; Woodward

and Clyde Consultants, 1986). This calculation gave ω values that were greater than 50 for both benzene and *p*-xylene, suggesting that the processes considered in this study may not be important on the field scale for these two compounds. As the tailing was underestimated in some of the curve fits, more experimental work is needed to state this conclusively. For more hydrophobic compounds and greater air flow rate, these processes may be important.

CHAPTER 6

CONCLUSIONS

The breakthrough curves obtained in this study indicated that micro-scale processes result in non-equilibrium conditions thus reducing the rate at which VOCs are removed via soil venting on the laboratory scale. The operative micro-scale processes were assumed to be slow reactions at sorption sites and slow aqueous phase intra-aggregate diffusion. Kinetic parameters obtained from the breakthrough curves suggest that equilibrium conditions will exist on the field scale for the processes studied.

Tailing of breakthrough curves was observed to increase with moisture content. This observation suggests that there are moisture-dependent processes that control the removal of VOCs. Two processes that have been suggested are inter- and intra-aggregate aqueous phase diffusion. This was confirmed using the fitted parameters obtained for the one-site kinetic model which gave rate coefficients that were found to be directly related to moisture content.

The one-site kinetic model is limited in that tailing is described solely in terms of slow reactions at binding sites. It does not account for slow aqueous phase diffusion. For this reason, the two-compartment model may give the best qualitative description if more than one slow process is operative. For this study, the two-compartment model did not provide any additional kinetic information.

The f_{oc} of the soil and the K_p values of benzene and *p*-xylene were relatively low. For a higher f_{oc} soil and compounds with high K_p values, tailing

may be entirely the result of slow reactions at the binding sites. In such systems, the one-site kinetic model could provide an accurate quantitative description.

APPENDIX A
OBSERVED AND FITTED HELIUM
BREAKTHROUGH CURVES

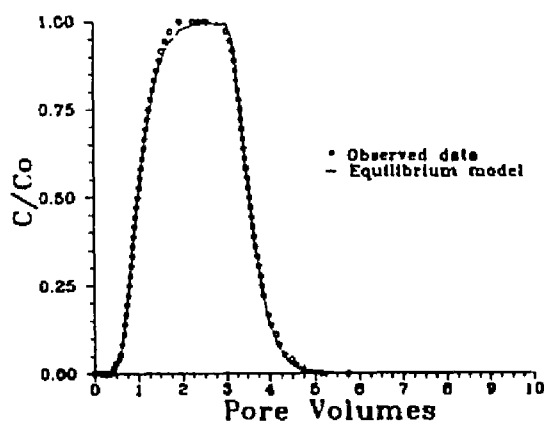


Figure A.1. Observed and fitted data for experiment H1W using the equilibrium model.

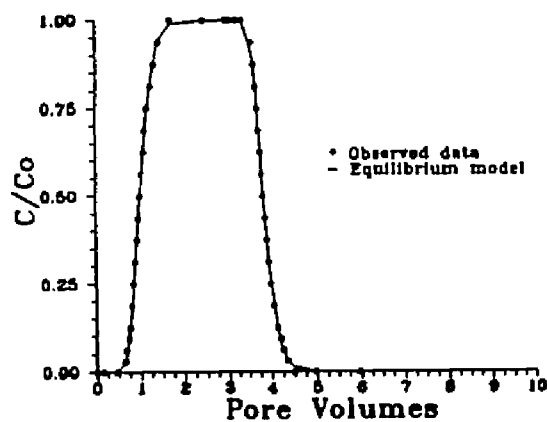


Figure A.2. Observed and fitted data for experiment H2W using the equilibrium model.

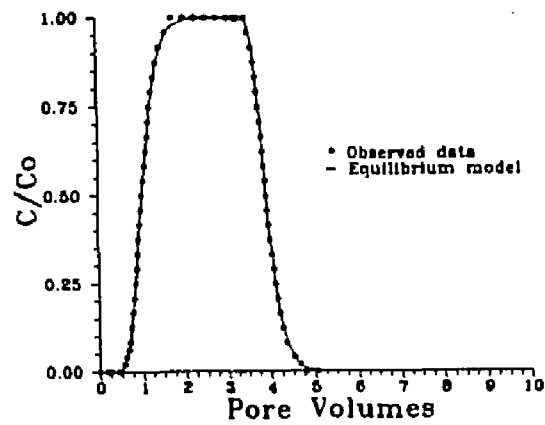
APPENDIX A--Continued

Figure A.3. Observed and fitted data for experiment H4W using the equilibrium model

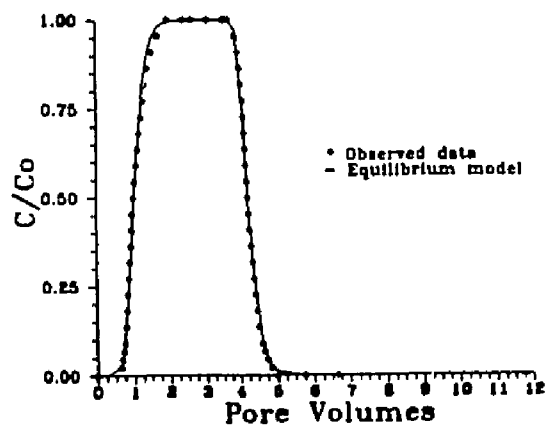


Figure A.4. Observed and fitted data for experiment H5W using the equilibrium model

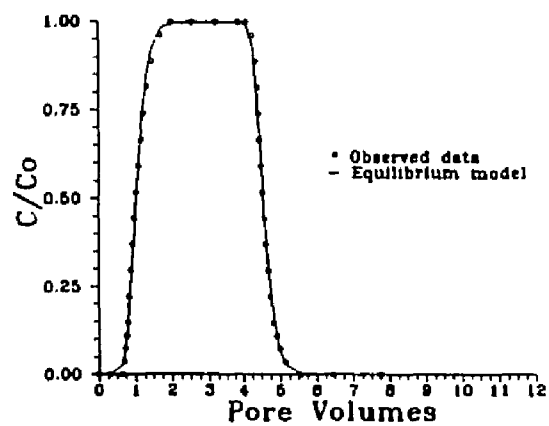
APPENDIX A--Continued

Figure A.5. Observed and fitted data for experiment H1D using the equilibrium model

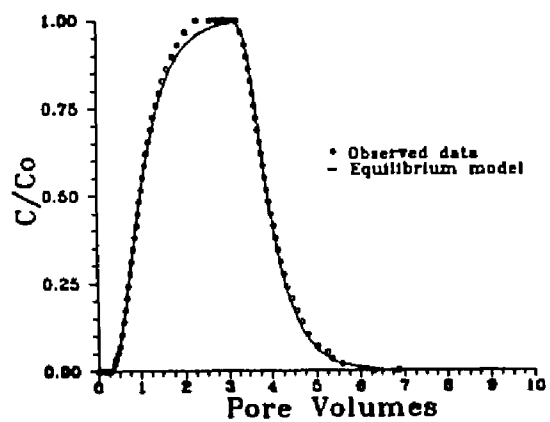


Figure A.6. Observed and fitted data for experiment H2D using the equilibrium model

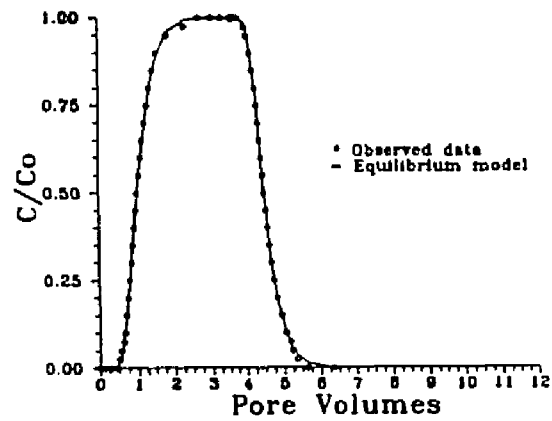
APPENDIX A--Continued

Figure A.7. Observed and fitted data for experiment H3D using the equilibrium model

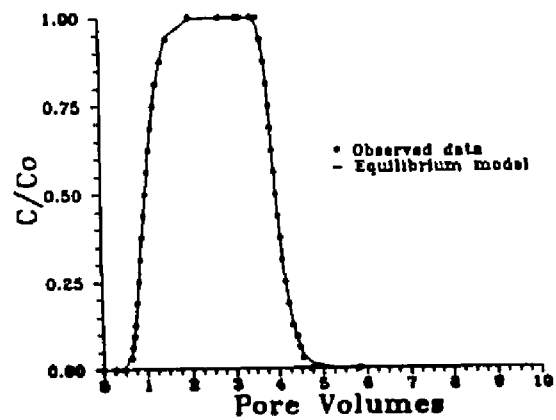


Figure A.8. Observed and fitted data for experiment H4D using the equilibrium model

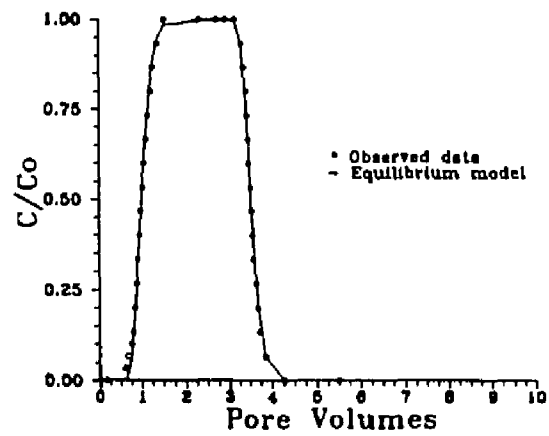
APPENDIX A--Continued

Figure A.9. Observed and fitted data for experiment H5D using the equilibrium model

APPENDIX B
OBSERVED AND FITTED BENZENE
BREAKTHROUGH CURVES

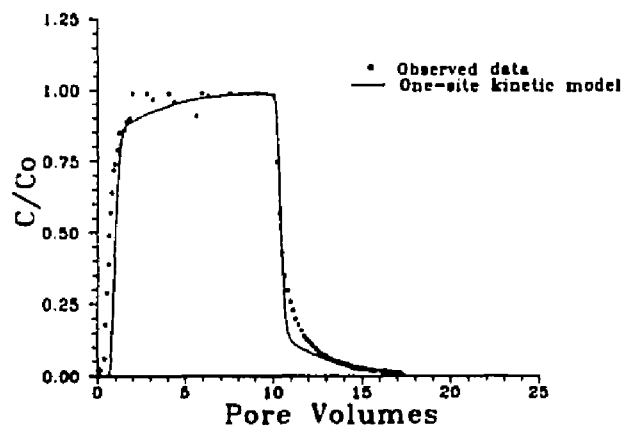


Figure B.1. Observed and fitted breakthrough curves for experiment B4 using the one-site kinetic model. R , T_1 , and ω were fitted by the program by CFITIM. P was fixed at 53.1.

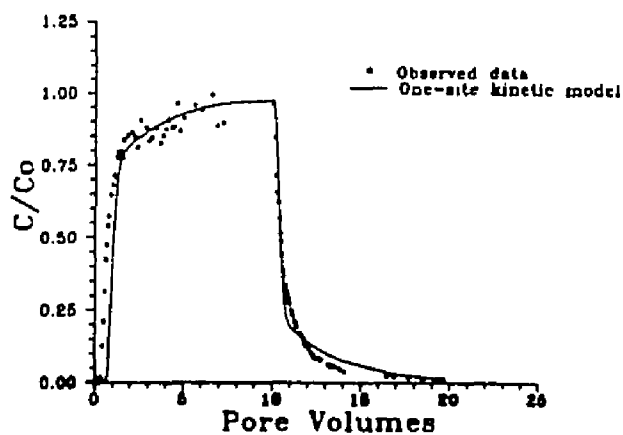


Figure B.2. Observed and fitted breakthrough curves for experiment B5 using the one-site kinetic model. R , T_1 , and ω were fitted by the program by CFITIM. P was fixed at 47.7.

APPENDIX B--Continued

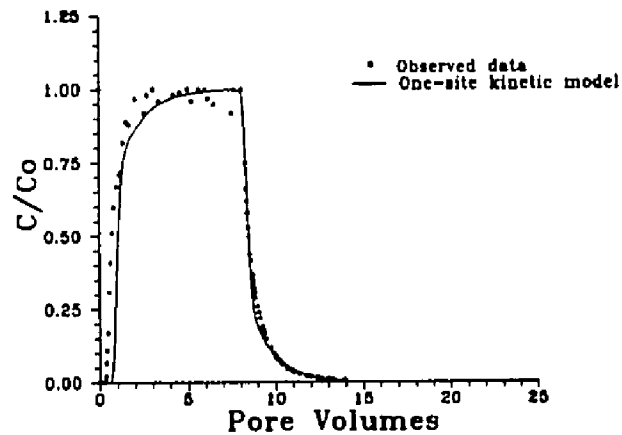


Figure B.3. Observed and fitted breakthrough curves for experiment B6 using the one-site kinetic model. R , T_1 , and ω were fitted by the program by CFITIM. P was fixed at 58.7.

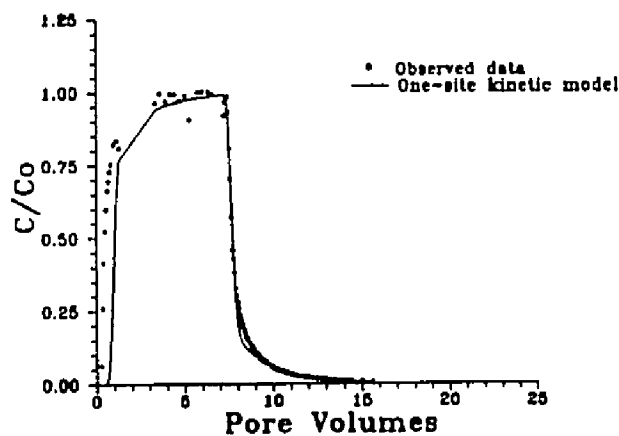


Figure B.4. Observed and fitted breakthrough curves for experiment B8 using the one-site kinetic model. R , T_1 , and ω were fitted by the program by CFITIM. P was fixed at 58.7.

APPENDIX B--Continued

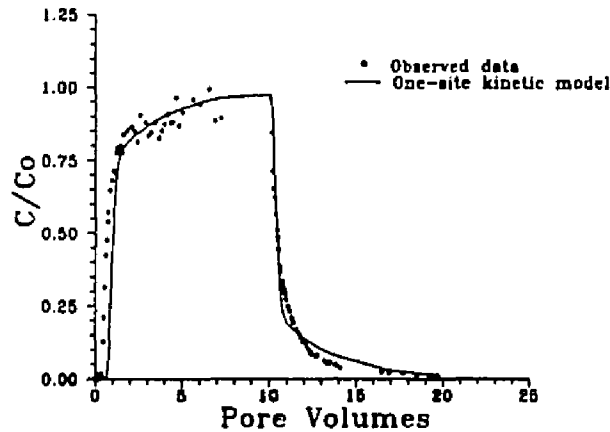


Figure B.5. Observed and fitted breakthrough curves for experiment B9 using the one-site kinetic model. R , T_1 , and ω were fitted by the program by CFITIM. P was fixed at 48.1.

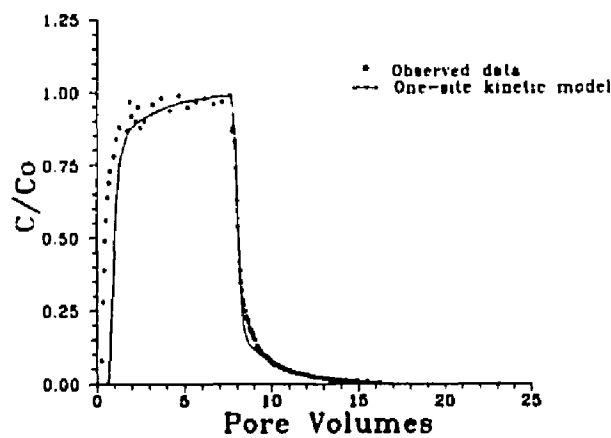


Figure B.6. Observed and fitted breakthrough curves for experiment B10 using the one-site kinetic model. R , T_1 , and ω were fitted by the program by CFITIM. P was fixed at 53.1.

APPENDIX B--Continued

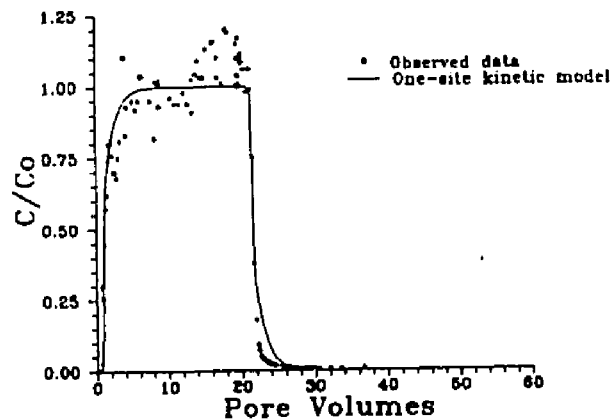


Figure B.7. Observed and fitted breakthrough curves for experiment B16 using the one-site kinetic model. R , T_p , and ω were fitted by the program by CFITIM. P was fixed at 71.5.

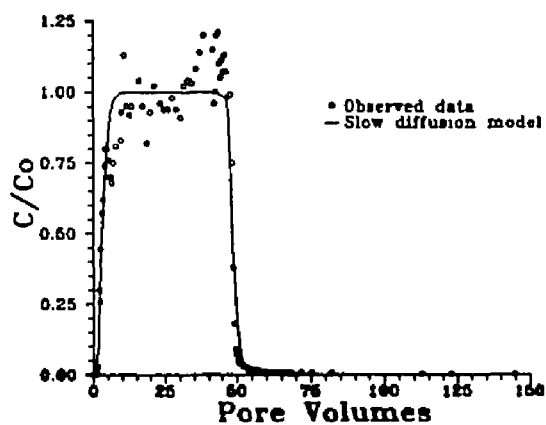


Figure B.8. Observed and fitted breakthrough curves for experiment B16 using the slow diffusion model. R , T_p , and ω were fitted by the program by CFITIM. P was fixed at 71.5.

APPENDIX C
OBSERVED AND FITTED *p*-XYLENE
BREAKTHROUGH CURVES

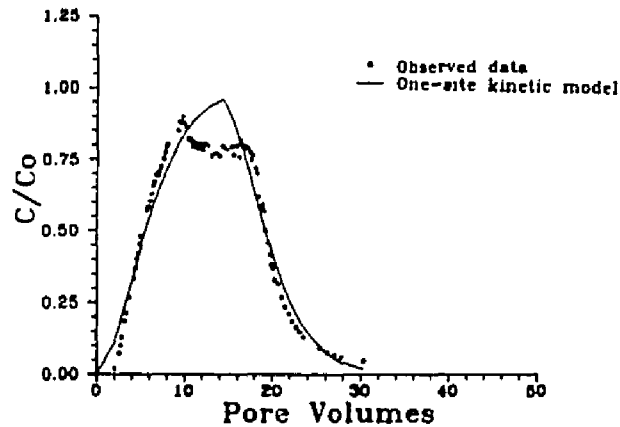


Figure C.1. Observed and fitted breakthrough curves for experiment XY8 using the one-site kinetic model. R , T_1 , and ω were fitted by the program by CFITIM. P was fixed at 54.1.

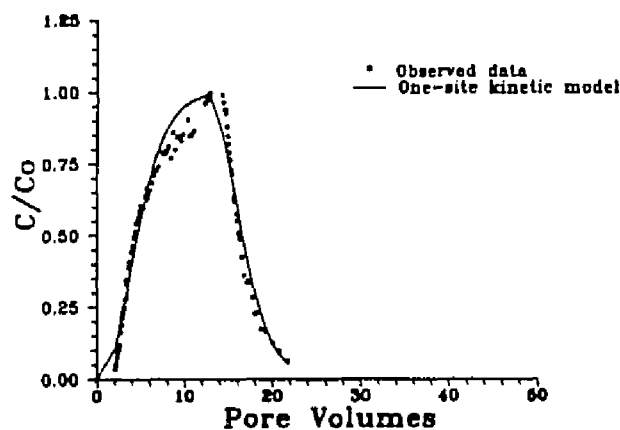


Figure C.2. Observed and fitted breakthrough curves for experiment XY10 using the one-site kinetic model. R , T_1 , and ω were fitted by the program by CFITIM. P was fixed at 60.3.

APPENDIX C--Continued

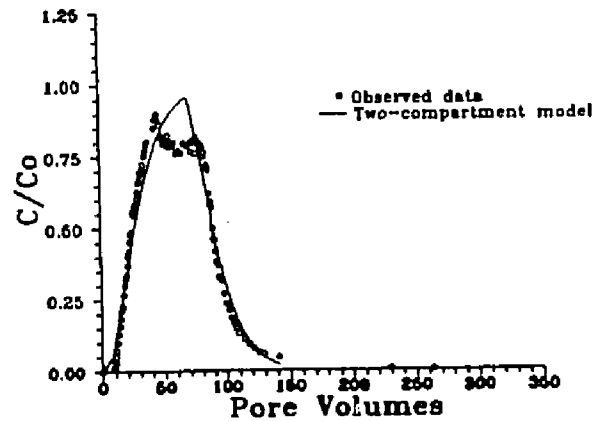


Figure C.3. Observed and fitted breakthrough curves for experiment XY8 using the two-compartment model. R , T_1 , ω , and β were fitted by the program by CFITIM. P was fixed at 54.1.

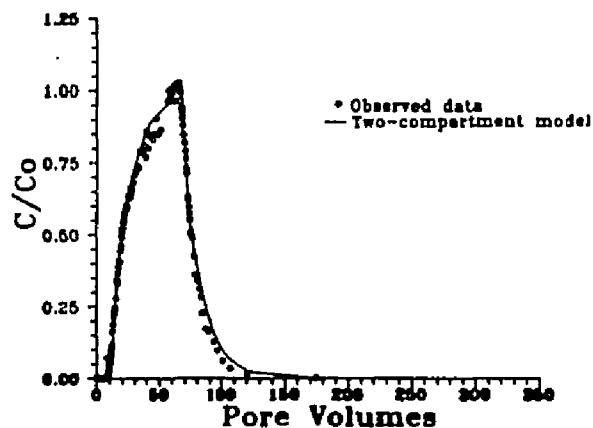


Figure C.4. Observed and fitted breakthrough curves for experiment XY10 using the two-compartment model. R , T_1 , ω , and β were fitted by the program by CFITIM. P was fixed at 60.3.

LIST OF REFERENCES

- Albertson, M., 1979, "Carbon dioxide balance in the gas-filled part of the unsaturated zone, demonstrated at a podzol", *Z. Pflanzenernaehr. Bodenkd.*, 142: 39-56.
- Bahr, J. and J. Rubin, 1987, "Direct comparison of kinetic and local equilibrium formulations for solute transport affected by surface reactions", *Water Resources Research*, 23: 438-452.
- Bear, J., 1979, *Hydraulics of Groundwater*, McGraw-Hill, Inc., New York, pp. 237-239.
- Bruckner, F., H.M. Harress, and D. Hiller, 1986, *Brunnenbau-Rohrleitungsbau*, 37: 174-179.
- Bruckner, F., and H. Kugele, 1985, "Sanierung von mit leicht-fluchtigen chlorierten Kohlenwasserstoffen (CKW) kontaminierten Boden mittels Absaugung der Bodenluft" ("Rehabilitation of soils contaminated by highly volatile chlorinated hydrocarbons (CHC) through withdrawal of soil air by suction"), *Korrespondenz Abwasser*, 32: 863-866.
- CRC, 1981-1982, *Handbook of Chemistry and Physics*, 62nd edition, (R.C. Weast and M.J. Astle, eds.), CRC Press, Boca Raton, Florida, 1981.
- Crow, W.L., E.P. Anderson, and E. Minugh, 1987, "Subsurface Venting of Vapors Emanating from Hydrocarbon Product on Ground Water", *Groundwater Monitoring Review*, Winter, pp. 51-57.
- Currie, J.A., 1970, "Movement of gases in soil respiration" in *Sorption and Transport Processes in Soils*, SCI Monogr., 37, Rothamsted Experimental Station, Harpended, England.
- Davis, J.H., 1989, *Sorption and Desorption of Benzene and p-Xylene on an Unsaturated Desert Soil*, (Unpublished M.S. Thesis), University of Arizona, Tucson, 141 pp.
- de Jong, E., and H.J.V. Schappert, 1972, "Calculation of soil respiration and activity from CO₂ profiles in the soil", *Soil Science*, 113: 328-333.
- De Smedt, F., and P.J. Wierenga, 1979, "A generalized solution for solute flow in soils with mobile and immobile water", *Water Resources Research*, 15: 1137-1141.

LIST OF REFERENCES--Continued

- Fischer, H.B., E.J. List, C.Y.R. Koh, J. Imberger, and N.H. Brooks, 1979, *Mixing in Inland and Coastal Waters*, Academic Press, Inc., Orlando, pp. 30-54.
- Freeze, R.A., and J.A. Cherry, 1979, *Groundwater*, Prentice-Hall, Inc., Englewood Cliffs, New Jersey, 604 pp.
- Grable, A.R., and E.G. Siemer, 1968, "Effects of bulk density, aggregate size and soil water suction on oxygen diffusion, redox potentials, and elongation of corn roots", *Soil Science Society American Proceedings*, 32: 180-186.
- Hillel, D., 1980, *Fundamentals of Soil Physics*, Academic Press Inc., Orlando, 413 pp.
- Karickhoff, S.W., D.S. Brown and T.A. Scott, 1979, "Sorption of Hydrophobic Pollutants on Natural Sediments", *Water Research*, 13: 241-248.
- Kilbury, R.K, T.C. Rasmussen, D.D. Evans, and A.W. Warrick, 1986, "Water and Air Intake of Surface-Exposed Rock Fractures in Situ", *Water Resources Research*, 22(10): 1431-1443.
- Lai, S.H., J.M. Tiedje and A.E. Erickson, 1976, "In situ measurement of gas diffusion coefficient through soil", *Soil Science Society American Proceedings*, 40(1): 3-6.
- Mackay, D. and W.Y. Shiu, 1981, "Critical review of Henry's law constants for chemicals of environmental interest", *Journal of Physical and Chemical Reference Data*, 10(4): 1175-1199.
- Marley, M.C., 1985, *Quantitative and qualitative analysis of gasoline fractions stripped by air, from the unsaturated soil zone* (M.S. Thesis), University of Connecticut, 87 pp.
- Marshall, T.J., 1959, "The diffusion of gases through porous media", *Journal Soil Science*, 10: 79-82.
- Millington, R.J., 1959, "Gas diffusion in porous media", *Science*, 130: 100-102.
- Penman, H.L., 1940, "Gas and vapour movements in the soil, 1, The diffusion of vapours through porous solids", *Journal of Agriculture Science*, 30: 437-462.
- Roberson, J.A. and C.T. Crowe, 1985, *Engineering Fluid Mechanics* (Third Edition), Houghton Mifflin Corp., Boston, 712 pp.

LIST OF REFERENCES--Continued

Schwarzenbach, R.P. and J. Westall, 1981, "Transport of Nonpolar Organic Compounds from Surface Water and Groundwater. Laboratory Sorption Studies", *Environmental Science and Technology*, 15: 1360-1367.

Szecsody, J.E. and R.C. Bales, "Sorption Kinetics of Low-Molecular-Weight Hydrophobic Organic Compounds on Surface-Modified Silica", *Journal of Contaminant Hydrology*, in press.

van Bavel, C.H.M., 1951, "A soil aeration theory based on diffusion", *Soil Science*, 72: 33-46.

van Genuchten, M. Th., 1981, *Non-equilibrium transport parameters from miscible displacement experiments*, Research Report No. 119, U.S. Salinity Lab, Riverside, California, 88 pp.

Welty, J.R., C.E. Wicks and R.E. Wilson, 1976, *Fundamentals of Momentum, Heat, and Mass Transfer* (Second Edition), John Wiley & Sons, New York, 789 pp.

Wesseling, J., 1962, "Some solutions of the steady state diffusion of carbon dioxide through soils", *Netherlands Journal Agricultural Science*, 10: 109-117.

Woodward and Clyde Consultants, 1986, Engineering report prepared for Siemens Components, Inc.

Wu, S-C., and P.M. Gschwend, 1988, "Numerical modeling of sorption kinetics of organic compounds to soil and sediment particles", *Water Resources Research*, 24(8): 1373-1383.